Neutrinos and Cosmic Rays Observed by IceCube

IceCube collaboration

present on four continents

Abstract

The core mission of the IceCube Neutrino Observatory is to study origin, propagation and properties of cosmic rays. IceCube with its surface component IceTop observes multiple signatures from cosmic-ray interactions to fullfil this mission. Neutrinos from cosmic-ray interactions in their sources as well as in interstellar space provide information about the origin and propagation of cosmic rays. The measurement of the muonic and electromagnetic component of air showers produced in the atmosphere enables measurements of the spectrum, composition and anisotropy of the local cosmic-ray flux. In this review we provide an overview of recent findings and their implications on our understanding of cosmic rays.

Keywords: IceCube, Neutrino, Cosmic Rays

1. Introduction

The first detection of high-energy neutrinos of cosmic origin in 2013 [1] by the IceCube Neutrino Observatory opened a new window onto the non-thermal processes in our universe. Neutrinos interact only weakly with matter, and can escape energetic and dense astrophysical environments that are opaque to electromagnetic radiation. Therefore, neutrinos promise to provide unique insights into a large number of extreme astrophysical phenomena, ranging from stellar explosions to the accretion on massive black holes. Moreover, at PeV energies, most of the universe is impenetrable to electromagnetic radiation, due to the scattering of high energy photons (γ rays) on the cosmic microwave background and other radiation fields.

This leaves neutrinos as the most important messengers to search for the origin of the highest energy cosmic rays (CR). High energy neutrinos are produced through the interaction of CR with ambient matter or radiation fields. Unlike the charged CR they are neither deflected by magnetic fields, nor affected by matter or radiation fields on the way from the source to the Earth. They propagate undisturbed over cosmic distances, allowing us to observe an otherwise opaque high energy universe and identify the sources in it.

Many candidate source classes exist that fulfill the basic requirements of accelerating CR to the highest observed energies of about 10^{20} eV. An upper limit on the reachable CR energy in gradual acceleration processes, like e.g. Fermi acceleration, was noted by Hillas in [2]. The size of the acceleration region has to be larger than the Larmor radius of the produced CR, otherwise the particles are not confined for further acceleration. This notion led to the famous plot that is shown in a modern adaption in figure 1. As can be seen, the potential sources of ultra-high energy CR are manyfold. They range from gamma-ray bursts (e.g. [3]), young neutron stars and pulsars (e.g. [4]), the jets (e.g. [5]) and cores of active Galaxies (e.g. [6]), to galaxy merger shocks in clusters (e.g. [7]).

IceCube's cosmic neutrinos can be used to probe the particle acceleration processes in these candidate source classes. Information can be deduced from the observed spectrum, the flavor composition and possible correlations of neutrino observations with known transients or sources. After a short introduction to the IceCube neutrino telescope in section 2, we summarize the findings and insights that have been obtained in the first five years of IceCube operation on the properties (section 3) and the origin of the cosmic neutrino flux (sections 4 – 6). In each section we will also discuss the implications of these findings for the sources of high-energy CR.

However, IceCube is more than ,,just" a cosmic neutrino detector. Using the surface array IceTop, and the thousands of muons from CR showers in the atmosphere that are registered every second in the in-ice array, IceCube can be used to study the spectrum, the composition and the isotropy of the CR that arrive at Earth at TeV and PeV energies.

At PeV energies a transition in the CR spectrum and composition has been observed by many instruments (see review in [9]). This so called CR ,,knee", is commonly attributed to Galactic sources being unable to accelerate CR to energies above a few PeV per nucleon. Consequently, the composition of CR changes at PeV energies, being dominated by increasingly heavier

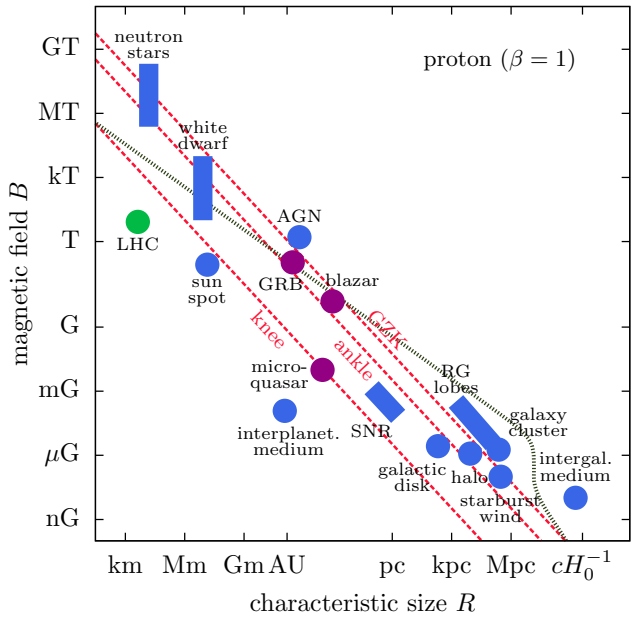

Figure 1: A modern adaption of the so called ,,Hillas plot" from [8]. It displays upper limits on the reachable CR energy dependent on the size of the acceleration region and magnetic field strength. The red lines indicate the upper limits due to the loss of confinement in the acceleration region for CRs at the *knee*, *ankle*, and the *GZK* cutoff. The dotted gray line corresponds to a second upper limit that arises from synchrotron losses in the sources and interactions in the cosmic photon background.

nuclei as the energy increases. The high statistics available in IceCube and the unique combination of a measurement of the electromagnetic and high-energy muon component of a CR air shower enable a precise measurement of both, spectral features and composition changes, in this interesting energy range.

Even though CR at TeV to PeV energies are efficiently deflected in the Galactic magnetic fields, the observation of small anisotropies in their arrival directions can give important clues on the existence and location of CR sources in our Galactic neighborhood. Such anisotropies have been observed by several instruments on the northern hemisphere [10, 11, 12, 13, 14, 15]. IceCube data now provide the most accurate measurement of this anisotropy in the Southern hemisphere at TeV and PeV energies, completing our picture of the arrival patterns of CR on the sky.

We summarize the spectrum and composition measurements in section 7, and show and discuss recent results of the IceCube anisotropy measurement

in section 8, before concluding this review in section 9

2. The IceCube neutrino observatory

The IceCube Neutrino Observatory at the South Pole instruments a gigaton of the deepest and cleanest South Pole ice. It has been taking data in full configuration since spring 2011 with a duty cycle of about 99%. With one cubic kilometer instrumented volume, IceCube is more than an order of magnitude larger than previous and current experiments operating in the North (Baikal Deep Under-water Neutrino Telescope, Antares). The planned KM3NeT and GVD detectors to be constructed in the Mediterranean sea and in the Lake Baikal in Siberia respectively, target a similar size as the one from IceCube [16, 17].

Optical sensors have been deployed at a depth between 1450 m to 2450 m below the glacial surface (see Fig. 2). In total, 5160 digital optical modules (DOMs) are attached to 86 cables (strings) in a 3D hexagonal array optimally arranged to detect the Cherenkov photons emitted by charged particles traversing the ice. IceCube consists of three components: the main IceCube array, the surface array IceTop, and a densely instrumented sub-array called DeepCore optimized for neutrinos with energies of a few tens of GeV. All the three components use the same instrumentation design of DOMs and associated electronic readout.

The primary array is composed of 78 strings with a vertical separation of the DOMs of 17 m and an inter-string distance of about 125 m. With this geometry, IceCube detects neutrinos from the entire sky and in the energy range of 10^{11} - 10^{16} eV. Primary CR interacting above the IceCube array, are detected with the CR air shower array IceTop that is operated in coincidence with the IceCube array. IceTop is composed of 162 water tanks filled with clear ice and arranged in pairs at stations on the surface. Each station is 25 m from the top of an IceCube string. Finally, DOMs have been also deployed in the center and deeper part of the IceCube array composing DeepCore, a denser instrumented volume optimally set to extend IceCube operation to the lower energy regime of 10 GeV. The vertical DOM-to-DOM spacing is 7 m and the inter-string spacing is 72 m and 42 m.

IceCube records events at a rate of about 2.5 kHz. The overwhelming majority of these events are muons from CR air showers that penetrate the ice and reach the depth of IceCube. Only about one in a million events is a neutrino. Yet, this is sufficient for the collection of an unprecedented large

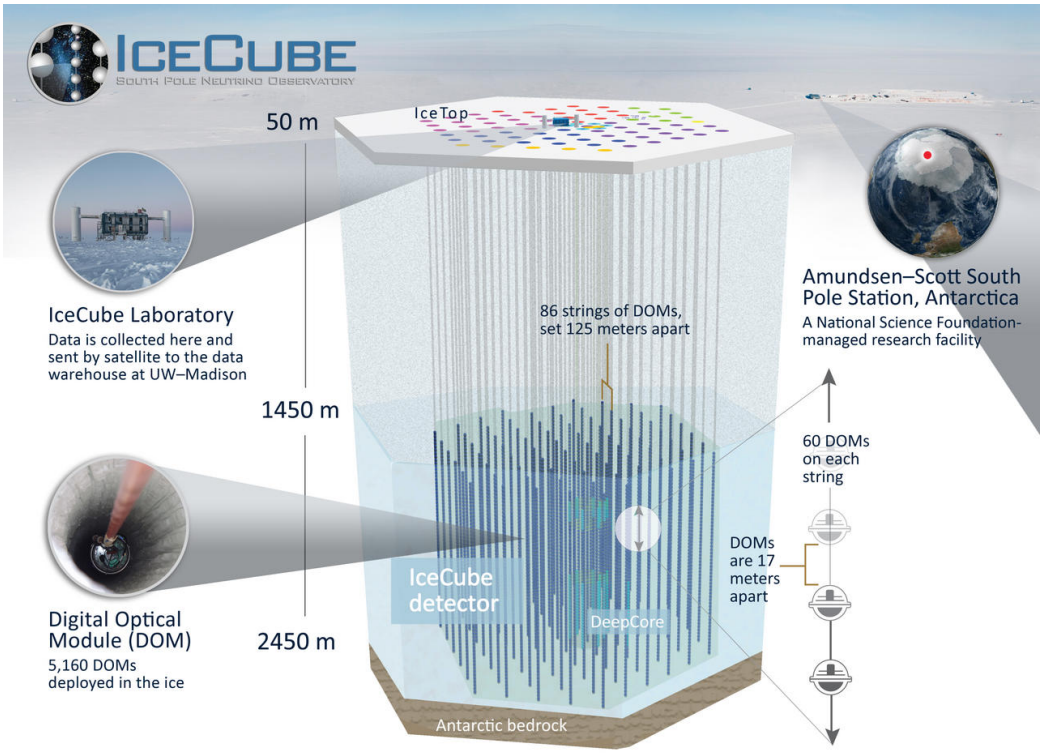

Figure 2: The IceCube Neutrino Telescope is composed of the IceCube array, the surface array IceTop, and the low energy sub-array called DeepCore.

sample of high-energy neutrinos ($\sim 10^5$ yr^{-1}) that offer a unique testbed for extreme astro- and particle physics.

Three main signatures can be distinguished for neutrino events in IceCube. Track-like events arise from muons produced in charged-current (CC) interactions of ν_μ. Shower-like events are generated in neutral-current (NC) interactions of all neutrino flavors, as well as in CC interactions of ν_e (all energies) and ν_τ (E $\leqslant$ 100 TeV). High-energy ν_τ can produce a specific identifying signature, the so called ,,double-bang" events. The hadronic shower at the τ generation vertex and the shower produced at the τ decay vertex can be separately identified when the tau track is longer than a few tens of meters ($\gamma c\tau_\tau \approx 50$ m at 1 PeV).

Figure 3 shows the propagation of Cherenkov photons in a simulation of the Antarctic ice for each described signature. Reconstruction of the physical

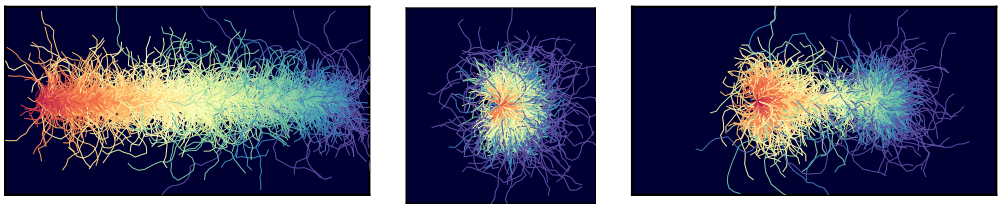

Figure 3: Propagation of Cherenkov light in the ice for typical event signatures observed by IceCube, a track-like event (left), a shower-like event (middle) and a double-bang event (right). Each track marks the path of a photon. The colors indicate the relative time of the photons with respect to each other. Early photons are red, late photons are blue.

properties of the neutrino that generated the event — direction, energy and flavor — is challenging due to the complex optical properties of the natural medium. Scattering and absorption in the ice mainly arises from deposits of minerals, soot and ash on the ice over several hundreds of thousands of years. Therefore both, scattering and absorption lengths vary strongly with depth. Additionally, the flow of the antarctic ice shield introduces an anisotropy to the scattering. Melting and refreezing of the ice during DOM deployment changes the optical properties locally. In particular for high energies above few tens of TeV the reconstruction of event properties in IceCube is therefore systematically limited. Shower-like events can be reconstructed with an energy resolution of $\sim 15\%$ [18], but the resolution of their arrival direction is poor, about 15°. The arrival direction of track-like events on the other hand can be reconstructed with an accuracy better than 1°, however the energy of the neutrino can only indirectly be inferred from the energy deposited in the instrumented volume.

IceTop is located at an altitude of 2835 m a.s.l. corresponding to an atmospheric overburden of 690 g cm^2. Each tank is instrumented with two DOMs operating at different gain to cover a dynamic range from about 1/6 VEM (vertical equivalent muon[1]) to 1140 VEM. The IceTop surface array is triggered when six tanks in three stations register a signal in coincidence. The signal in the triggering tanks is typically dominated by the electromagnetic component of air showers. For each trigger, both the surface detector and the in-ice signal are read out. IceTop has a small, central in-fill array with

[1]The energy deposited by a minimally ionizing muon traversing the tank in vertical direction.

a threshold of about 100 TeV primary CR energy, and the regular spaced array with a threshold of 300 TeV. It records air showers from primary CR of energies up to about 2 EeV above which the rate becomes too low for analysis. The direction of events is reconstructed from the shower front arrival time with a resolution of $\sim 0.3^\circ$ at 10 PeV. The shower energy is determined by fitting the lateral shower profile and using the signal size at a perpendicular distance from the shower core of 125 m. The resolution for protons at 30 PeV energy is 0.05 in $\log_{10}(\mathrm{E/GeV})$ [19].

3. Spectrum and flavor composition of astrophysical neutrinos

The majority of the neutrino events detected by IceCube are produced in the atmosphere. The first strong evidence for a cosmic neutrino component came from a search for cosmogenic neutrinos using data from May 2010 to April 2012 [20]. Two events with energies above 1 PeV were discovered, both cascades starting inside the detector. A follow-up search of the same data for events starting in the detector with more than $\simeq 30$ TeV deposited energy found 27 high-energy events [1], including the two PeV events. The spectrum and zenith angle distribution of the events was incompatible with the hypothesis of atmospheric origin on a $> 4\sigma$ level.

Since then, IceCube collected independent evidence for an astrophysical neutrino signal by analyzing different event signatures, including shower-like and starting events at lower energies as well as track-like events that interact outside the detector (called through-going events).

3.1. Starting Events

Neutrino interactions are identified by searching for an interaction vertex inside the instrumented volume. This search is sensitive to both shower-like and track-like events. Since the main background for this search is comprised of muons from CR air showers, the rejection strategy is to identify Cherenkov photons from a track entering the detector. For that the outer parts of the instrumented volume are assigned to a ,,veto" region and an event is rejected if a certain number of Cherekov photons are found in this veto region that precede the photons produced at the interaction vertex. For a more detailed description see [21]. So far data recorded between May 2010 and Apr 2014 have been analyzed to obtain a starting event sample with an energy threshold of $\mathrm{E}_\nu \sim 30$ TeV [22] including three shower-type events with energies in excess of 1 PeV. If the size of the veto region is chosen

to increase as energy decreases, neutrino induced shower-like and track-like events above a few TeV can be isolated from the background effectively. Using this approach, the starting event sample for two years (May 2010 to April 2012) has been extended to include lower-energy events down to $E_\nu \sim 3$ TeV [23].

3.2. Shower-type events

An alternative strategy to distinguish neutrino-induced shower-type events from atmospheric backgrounds is to search for a spherical light pattern that fits the characteristics of Cherenkov light emission from a short[2] and well localized particle shower in or around the instrumented area. This allows identification of showers from neutrino interactions also in regions of the instrumented volume that serve vetoing purposes in the starting event searches and even to find showers nearby the instrumented volume. Data from May 2010 to Apr 2012 has been analyzed using this technique [24] selecting 172 shower-type events above $E_\nu \sim 10$ TeV. Most of these events are different from the starting events of the same time period.

3.3. Through-going muons

Muons produced in CC neutrino interactions far outside the detector can still reach the instrumented volume to produce track-like events. Even a 1 TeV a muon can penetrate several kilometers of ice before it stops and decays. This allows observation of high-energy neutrino interactions from a much larger volume than the instrumented one, thereby increasing the effective area of the detector substantially. However, these so called through-going muons from neutrino interactions are indistinguishable from single high-energy muons produced in atmospheric showers. For this reason the Earth must be used as a filter to separate neutrino-induced from CR-induced muons: Muons that arrive from zenith angles above $\sim 85^\circ$ must be produced in neutrino interactions, as muons produced in CR air showers could not penetrate far enough through the Earth and ice to reach the detector. The spectrum of neutrino-induced, upward muons shows a hardening above the steep atmospheric background consistent with an astrophysical flux [25]. The search for such muons has recently been extended to 6 years of IceCube data

[2]For O(100 TeV) hadronic and electromagnetic showers there is only a few meters distance between interaction vertex and shower maximum in ice, which is small compared to the typical distance between strings of 125 m.

recorded between May 2009 and April 2015. The highest energy track found in this sample deposited 2.6 PeV of energy inside the volume of IceCube.[26]. The search for through-going muons is sensitive to cosmic neutrinos above an energy of about $E_\nu \sim 200$ TeV. At lower energies muons from the interactions of atmospheric ν_μ dominate over the cosmic component.

3.4. Showers from ν_τ interactions

An attempt was made to identify ν_τ interactions in the IceCube data recorded between May 2010 and Apr 2013, searching for a double pulse signature within single optical modules that would be characteristic of a double shower from the interaction and the decay vertices of the tau [27]. No such signature was found in 3 years of IceCube data, which is compatible with 0.54 expected events from simulations, if cosmic neutrinos arrive at Earth with a flavor ratio of $\nu_e : \nu_\mu : \nu_\tau = 1 : 1 : 1$. While no ν_τ signature was detected the analysis helps to constrain the measurement of this flavor ratio in combination with the observation channels introduced above.

3.5. Combined results

The combined analysis of available IceCube data analyzed until 2015 from all detection channels[3] results in a spectrum above 20 TeV consistent with an unbroken power law with best-fit spectral index of -2.49 ± 0.08 [28]. A slightly improved likelihood is obtained if the data is fitted with a harder spectrum with a spectral index of -2.31 and an exponential cutoff at 2.7 PeV, but the improvement is not significant enough ($\sim 1.2\sigma$) to claim the existence of such a cutoff. Both spectral models can describe the data reasonably well. However, the most recent analysis of high-energy muon tracks above 200 TeV prefers a spectral index of -2.13 ± 0.13 [26]. This result may be indicative of a spectral hardening (see figure 4) at high energies.

The energy flux of cosmic neutrinos above 10 TeV is 6.8×10^{-10} ergs cm^{-2} s^{-1} sr^{-1}. This is of the same order of magnitude as the energy flux of gamma rays above 10 GeV, and of CR above 10^{19} eV. The spatial distribution of events on the sky is compatible with an isotropic distribution of sources, suggesting an extragalactic origin of a substantial fraction of the observed cosmic neutrinos. Using the combined analysis, also the flavor ratio of the

[3]Through-going muons are only included from the data taking periods between May 2009 and Apr 2012. An additional 3 years of through-going muons were analyzed only after the publication of the combined analysis. See also Fig. 4.

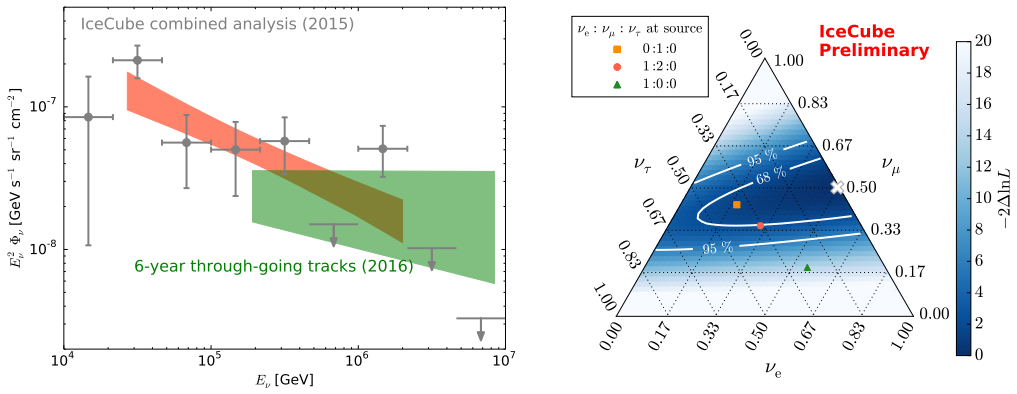

Figure 4: Left: Spectrum of cosmic neutrinos measured in a combined analysis of all detection channels (grey points, red bar). A new measurement based on 6 years of through-going muons (green bar) that is sensitive at higher energies indicates a harder spectrum above few hundred TeV. Right: Flavor constraints on the cosmic neutrino flux from the combined analysis in comparison to different scenarios expected for neutrino production in astrophysical sources.

observed cosmic neutrinos can be constrained. Figure 4 shows the constraints on the relative contributions of the individual neutrino flavors to the cosmic neutrino flux. Typical astrophysical scenarios expect a flavor ratio at the production site of $\nu_e : \nu_\mu : \nu_\tau = 1 : 2 : 0$ in case the neutrinos are produced by the decay of pions. Neutrino oscillations change this into $\nu_e : \nu_\mu : \nu_\tau \approx 1 : 1 : 1$, when they arrive at Earth. If the secondary muons loose most of their energy before they can decay, e.g. due to strong magnetic fields in the sources, the production flavor ratio would be $\nu_e : \nu_\mu : \nu_\tau = 0 : 1 : 0$ („muon-damped" scenario). In case the neutrinos are produced in the decay of neutrons a $\nu_e : \nu_\mu : \nu_\tau = 1 : 0 : 0$ flavor ratio would be expected. Figure 4 indicates the expected flavor ratios at Earth from these scenarios. The neutron decay origin is excluded at more than 3σ confidence, while both the standard and „muon-damped" production scenarios are compatible with the observations.

4. Neutrino sources

4.1. Search for individual neutrino sources

In case the cosmic neutrino flux is dominated by bright sources, individual neutrino sources should be detectable as a local excess of events on the

sky with respect to the atmospheric neutrino and diffuse cosmic neutrino background. The sensitivity of a search for such features depends crucially on the precision by which the direction of the neutrinos can be reconstructed from the data, i.e. on the detector angular resolution.

Therefore, the best event signatures for this search are the through-going muons and track-like starting events with median angular resolutions of $\sim 0.5^\circ$ and $\sim 1^\circ$ respectively (at 100 TeV). The starting events are particularly important for the analysis of the Southern hemisphere where the strong background of muon bundles from CR air showers requires a very high energy threshold for the acceptance of through-going tracks.

The most recent analysis combines seven years of IceCube data recorded between May 2008 to Apr 2015, corresponding to a livetime of 2431 days of through-going muons, and 1715 days of track-like starting events[4]. In total 422791 through-going muons from the Northern hemisphere, 289078 through-going muons from the Southern hemisphere and 961 starting tracks have been collected. The overwhelming majority of the muons from the North originate from atmospheric neutrinos, while most of the muons from the South arise from muons and muon bundles created in CR air showers. The acceptance of background events vs. signal neutrinos has been optimized to achieve optimal sensitivity for a point source detection for a range of potential source spectra. The datasets are analyzed using a maximum likelihood technique to find one or more localized excesses over the diffuse backgrounds that correspond to point sources of neutrinos.

Figure 5 presents the discovery potential for point sources at various declinations δ that is achieved in this analysis. Shown is the neutrino flux from a point source over half a decade in energy that would lead to a 5σ discovery for 50% of statistical realizations. The most sensitive energy range changes with declination and is > 1 PeV for $\delta = -60^\circ$, between 100 TeV and 1 TeV at the horizon, and below 100 TeV at $\delta = 60^\circ$. The dashed line shows the sensitivity if starting events would be ignored, underlining their importance for Southern hemisphere point source searches. The generally lower discovery potential for sources at $\delta = -60^\circ$ is due to the limited overburden of ice above the detector which limits the amount of neutrino interaction tar-

[4]Starting events were not available for in-construction IceCube before May 2010. The through-going muon sample contains data from the partially completed IceCube detector in its 40 and 59 string configurations.

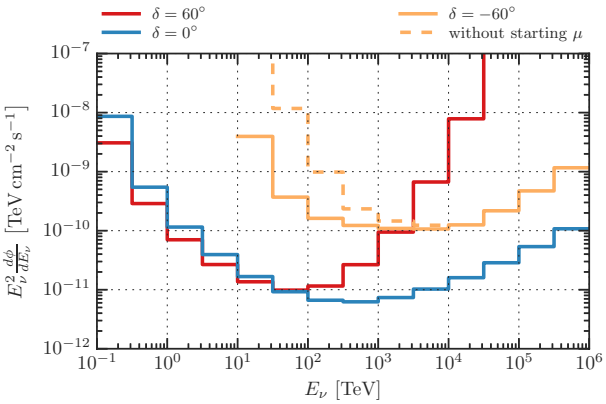

Figure 5: Differential discovery potential of the point source search for various zenith angles. Shown is the neutrino flux form a point source over half a decade in energy that would lead to a 5σ discovery in the current search for 50% of statistical realizations. A power-law spectrum with an index of 2 is assumed for the neutrino flux within a single energy bin.

get material, and the high-energy threshold for accepting muons to reduce the strong background from CR air showers. For sources at a declination of $\delta = 60°$, neutrinos with energies $> 100\ TeV$ are increasingly absorbed in the Earth, reducing the discovery potential at high energies.

4.2. Flux upper limits derived from IceCube data

No indication for a neutrino point source has been found in the IceCube data so far. Figure 6 summarizes the results of the search described above. The map shows the p-values for each point in the sky giving the local probability that an excess is a fluctuation of the background. To estimate the significance of the lowest observed p-values on each hemisphere, event samples have been generated with the right ascension coordinates randomized. These samples have been analyzed in the same way as the original dataset. The distribution of the minimum p-values in the samples can then be compared to the one observed in the data. The fraction of randomized samples with a lower p-value than the lowest observed p-value is 29% for the Northern sky, and 17% for the Southern sky, i.e. the observations are compatible with fluctuations of the diffuse background.

Additonally, the known locations of individual promising neutrino source candidates have been tested. These candidates have been selected based on

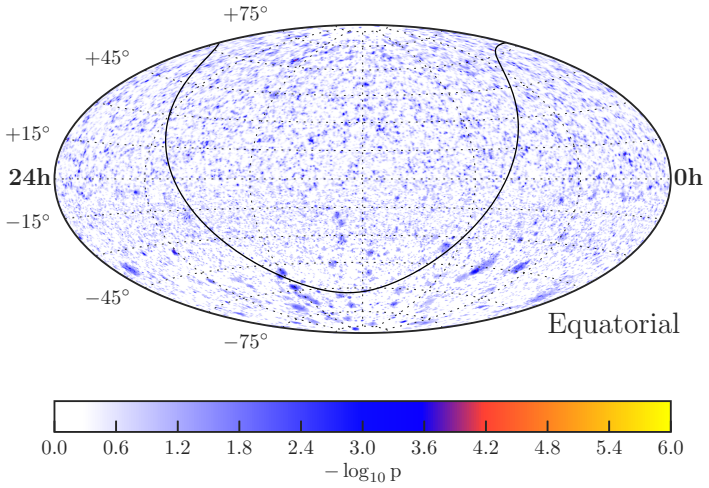

Figure 6: Map of p-values that an excess of events at a given position in the sky is due to a fluctuation of the background [29].

model calculations and/or the observation of non-thermal emission features in the electromagnetic spectrum. For none of the tested candidates a significant excess of neutrino events around their position has been observed. In figure 7 the neutrino flux upper limits are summarized that result from this non-observation. The red dots indicate the 90% CL flux upper limits for individual candidate sources. The dashed red line represents the corresponding sensitivity at the respective declination. Also given is the discovery potential, i.e. the flux that would lead to a 5σ discovery in 50% of statistical representations (without any corrections for multiple trials). The blue line represents the flux upper limit that corresponds to the lowest observed p-value in each half of the sky as a function of declination (the actual declination of the observed spots is indicated by a star).

A comparison of the obtained flux upper limits to individual source models is shown in figure 8. The flux limits have to be calculated specifically for the predicted neutrino spectra, based on the declination and energy dependent instrument response. The two panels show examples of recent models of the neutrino emission from Blazars [31, 32]. The predicted spectra are compared to the flux upper limits derived from IceCube data. For some of the sources the limits are on the level of the calculated flux starting to constrain the parameter space of such models.

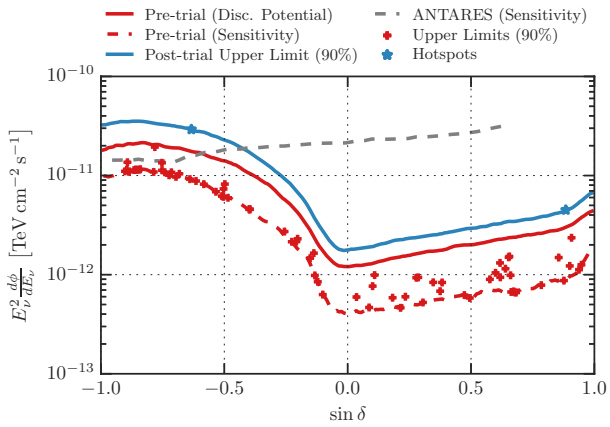

Figure 7: Neutrino flux upper limits for various source candidates, sensitivities and discovery potential as a function of the source declination (see text for details). The gray dashed line indicates the sensitivity of the Antares neutrino telescope [30]. A power-law spectrum with an index of 2 is assumed when generating the limits.

More details about the search presented above can be found in [29]. In addition, dedicated tests were performed to find transient sources [33] or sources that are spatially extended [34][5], also yielding null results.

4.3. Constraints on astrophysical source populations

The observation of an isotropic flux of astrophysical neutrinos seems to be at odds with the non-observation of individual neutrino point sources in the same data [35, 36, 37, 33, 30, 38, 39, 29]. However, the two results are consistent if the diffuse flux is dominated by many weak sources that are individually below the point-sources sensitivity [40, 41, 42]. This argument can be turned into a lower limit on the abundance of extra-galactic neutrino sources, that we outline in the following.

The (quasi-)diffuse flux of neutrinos ϕ (in units of GeV^{-1} s^{-1} cm^{-2} sr^{-1}) originating in multiple cosmic sources is simply given by the redshift integral [43]

$$\phi_\nu(E_\nu) = \frac{c}{4\pi} \int_0^\infty \frac{\mathrm{d}z}{H(z)} \mathcal{Q}_\nu(z, (1+z)E_\nu)\,. \tag{1}$$

Here, $H(z)$ is the red-shift dependent Hubble expansion rate and $\mathcal{Q}_\nu$ is the

[5]This searches so far did not use the full May 2008 – Apr 2015 dataset described above.

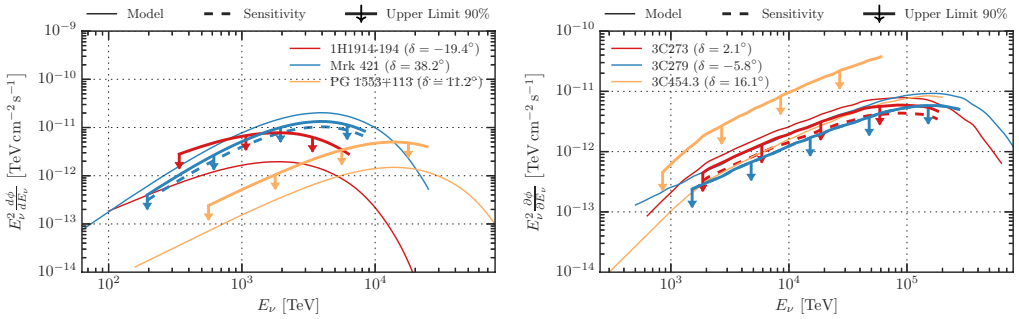

Figure 8: Limits on Blazar models.

spectral emission rate density of neutrinos. To a first approximation, we decompose the emission rate density into $\mathcal{Q}(z, E) = \rho(z)Q_\nu(E)$ where ρ is the source density and Q_ν is the emission rate per source. Note, that this approximation assumes that neutrino sources are *standard candles* and does not allow for luminosity distributions. However, these aspects can be included in a more detailed treatment.

The Hubble expansion in the red-shift integral of Eq. (1) limits the contribution of sources beyond the Hubble horizon c/H_0. The red-shift dependence of the source distribution can then be parametrized by the energy dependent quantity

$$\xi_z(E) = \int_0^\infty \mathrm{d}z \frac{H_0}{H(z)} \frac{\mathcal{Q}_\nu(z, (1+z)E)}{\mathcal{Q}_\nu(0, E)}\,, \tag{2}$$

which is typically of $\mathcal{O}(1)$. For the special case of power-law spectra $\mathcal{Q}_\nu(E) \propto E^{-\gamma}$ this quantity becomes energy independent and, for simplicity, we will assume the case $\gamma = 2$ in the following. For instance, we have $\xi_z \simeq 2.4$ if we assume that the source evolution follows the star-formation rate (SFR) [44, 45] or $\xi_z \simeq 0.5$ for a source distribution with no evolution in the local ($z < 2$) Universe.

Based on the observed per-flavor diffuse flux at the level of $E^2\phi_\nu \simeq 10^{-8}$ GeV^{-1} s^{-1} cm^{-2} sr^{-1} we can then estimate the average neutrino point source luminosity via Eq. (1) as $E^2Q_\nu(0, E) \simeq (4\pi H_0/c\xi_z\rho_0)E^2\phi_\nu$. On the other hand, for a homogeneous source distribution ρ_0 in the local Universe we expect that the brightest source contributes with a flux $E^2\phi_\nu^{\mathrm{PS}} \simeq 0.55(f_{\mathrm{sky}}\rho_0)^{2/3}E^2Q_\nu$ where $f_{\mathrm{sky}} \leq 1$ is the effective sky coverage of the observatory (see Ref. [43] for details). This translates into a point source

flux

$$E^2\phi_\nu^{\rm PS} \simeq 3.4\times10^{-12}\left(\frac{\xi_z}{2.4}\right)^{-1}\left(\frac{f_{\rm sky}}{0.5}\right)^{\frac{2}{3}}\left(\frac{\rho_0}{10^{-8}{\rm Mpc}^{-3}}\right)^{-\frac{1}{3}}\frac{\rm TeV}{\rm cm^2\,s}\,. \quad (3)$$

Presently, the sensitivity of IceCube of continuous point source emission in the Northern Hemisphere is at the level of $E^2\phi^{\rm PS}_{\nu_\mu+\bar\nu_\mu}\sim10^{-12}$ TeV cm^{-2} s^{-1} (see section 4.2 and figure 7), which is already putting some tension on very rare source candidates like blazars ($\rho_0\lesssim10^{-7}$ Mpc^{-3}). In fact, a dedicated analysis of the IceCube collaboration looking for the combined neutrino emission of Fermi LAT identified blazars [46] places an upper limit on their contribution that is at the level of about 25% of the observed flux. Figure 9 shows the maximum contribution from Blazars in the 2LAC catalog to the observed cosmic neutrino flux for two different spectral hypotheses. If additionally a strict proportionality is assumed between the emitted power at GeV energies and in TeV neutrinos, the 2FGL Blazars can contribute less than 10% to the observed flux (e.g. for sources for which the high-energy emission is dominated by pion-decay processes).

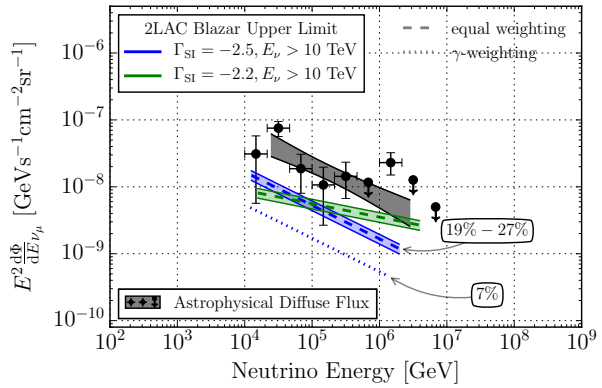

Figure 9: Upper limit on the contribution of Fermi LAT observed Blazars (2LAC catalog) to the cosmic neutrino flux. The upper limit is shown for two different power-law spectra for the neutrino flux with indices of 2.5 and 2.2, respectively. The width of the upper limit band indicates how the upper limit depends on the relative distribution of neutrino luminosities in the Blazar sample, if no strict proportionality is assumed between the γ-ray and neutrino luminosity of the source. The dashed lined indicates the upper limit in case such proportionality is considered.

A similar line of arguments can also be applied to transient sources [43]. Here, the experimental livetime does not increase the individual emission of

transients, but the total size of the source sample with local burst density $\dot{\rho}_0$. For instance, the contribution of gamma-ray bursts ($\dot{\rho}_0 \simeq 10^{-9}$ Mpc^{-3} yr^{-1}) to the diffuse emission is limited to less than 10% due to strong IceCube's limit on the prompt neutrino emission of GRBs coincidence with the gamma-ray signal [37].

4.4. Neutrinos from the propagation of UHECR

The CR spectrum extends to energies far above 10^{18} eV. These ultra-high energy (UHE) CR are believed to be accelerators in extra-galactic sources since Galactic magnetic fields are too weak to sufficiently confine the UHE CR. Candidate sources include gamma-ray bursts, active galactic nuclei or galaxy clusters (see Fig. 1).

The propagation of UHE CRs over cosmic distances makes them susceptible to interactions with cosmic backgrounds. In particular, photo-pion production of CR nuclei with the cosmic microwave background (CMB) with a local density of about 410 cm^{-3} becomes resonant at CR nucleon energies of about 7×10^{11} GeV. This leads to a strong suppression of CR protons beyond an energy at about $E_{\rm GZK} \simeq 5 \times 10^{19}$ eV, which is known as the Greisen-Zatspin-Kuz'min (GZK) suppression [47, 48].

The neutrinos from the decaying pions are the so-called *cosmogenic* or *GZK* neutrinos [49]. For proton-dominated UHE CR models the expected flux peaks at EeV energies and is expected to be equally distributed between neutrino flavors after propagation [50, 51, 52]. This flux is considered a *guaranteed* contribution to high-energy neutrino fluxes since it does not rely on specific neutrino production mechanisms in CR sources. However, even in the simplest case of proton-dominated models the flux depends on the unknown UHE CR redshift luminosity function and maximal energy cutoff of the proton spectra.

The largest contribution are predicted in proton models with a low cross-over between Galactic and extragalactic CRs which typically requires a strong redshift evolution of sources to fit the data [53, 54, 55, 56]. However in this case the related production of high energy gamma-rays, electrons and positrons predict a strong extragalactic diffuse gamma-ray background [57, 58, 59, 60, 61, 62] in excess of observations with Fermi LAT [63, 64].

Proton-dominated UHE CR models generally provide the most optimistic predictions for cosmogenic neutrino fluxes and are in reach with present neutrino observatories. However, the large experimental uncertainties of the relative contribution of elements translates into large uncertainties in the

GZK neutrino predictions. The reason is simple. If the UHE CR spectrum is dominated by heavy nuclei with atomic mass number A the resonant interaction of CR nucleons with the CMB is shifted to higher CR energies, $(A/56) \times 4 \times 10^{13}$ GeV. For the extreme case of iron this would shift the required CR energies to a level which is beyond the observed CR spectrum and GZK neutrino predictions are hence not supported by CR data.

Due to this increased threshold of GZK neutrino production of heavy nuclei additional cosmic radiation backgrounds with higher photon energies can become a more important target. The extragalactic background light (EBL) in the infrared, optical and ultra-violet are included in most GZK neutrino predictions including heavy nuclei [65, 66, 67, 68, 69, 70, 71, 60, 72]. In general these EBL neutrino predictions shift the peak neutrino production to the 1-10 PeV range but at an absolute level that is beyond present experimental sensitivities. As in the case of the proton dominated model the cosmogenic neutrino prediction depends also on maximal energies and evolution of models. An estimate of a lower limit of these pessimistic models was given in Ref. [73].

The search for cosmogenic neutrinos is one of the standard analyses of IceCube. At EeV energies, where the emission is expected to peak, there are practically no background events from atmospheric CR interactions. However, even after seven years of observation, no signal consistent with the expected emission spectra of various GZK models have been detected [74]. These limits now start to exclude some of the more optimistic scenarios of UHE CRs, dominated by light nuclei and/or strong source evolution (see also Ref. [61]).

5. Neutrino transients

5.1. Gamma-Ray Bursts

Gamma-Ray Bursts (GRBs) are short γ-ray flashes lasting from fractions of a second to tens of minutes. During their prompt emission they are the brightest explosions in the Universe reaching isotropic-equivalent energies of up to 10^{54} ergs likely powered by the core-collapse of a very massive star or the merger of two compact objects. Their locations are distributed isotropically and they have been measured up to a redshift of eight. GRBs have been proposed as the sources of the highest-energy CR. The central engine produces highly relativistic collimated jets, which are predicted to host internal shocks, where particles are efficiently accelerated to high energies. In

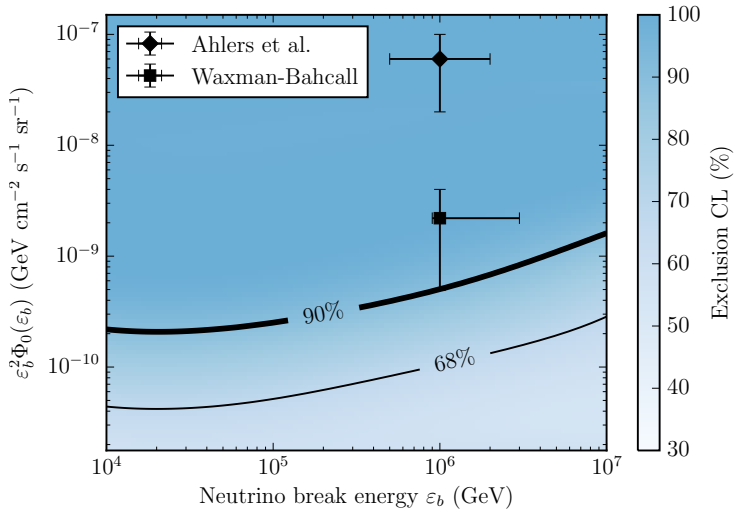

Figure 10: Limits on GRB model parameters adopted from Aartsen et al. [75].

hadronic scenarios accelerated protons interact with ambient synchrotron photons and produce high-energy neutrinos. The neutrino emission is expected to be collimated and in temporal coincidence with the prompt γ-ray emission.

A search for high-energy neutrinos detected by IceCube from the locations of 807 GRBs in coincidence with their prompt γ-ray emission did not find a significant excess compared to background expectations [75]. This result allows us to set tight constraints on models of neutrino and ultra-high-energy CR production in GRBs. Current models assuming CR escape via protons [3] and models assuming CR escape via neutrons [76] are excluded at 90% confidence (see Figure 10). However, models assuming multiple emission regions predict a neutrino flux below our current sensitivity [77].

Limits on the neutrino flux normalization allow us to constrain the contribution of γ-ray bright GRBs to less than 1% of the observed diffuse neutrino flux [78]. However, a possibly large population of choked-jet GRBs with low γ-ray luminosity might contribute a larger fraction of the diffuse flux. Choked jets may explain transrelativistic supernovae (SNe) and low-luminosity GRBs, giving a unified picture of GRBs and GRB-SNe [79]. This scenario can be tested by correlating high-energy neutrinos with SNe.

5.2. Supernovae

Analogous to GRBs, high-energy neutrino production is predicted from SNe hosting mildy relativistic jets, which get choked in the envelope of the star [80, 81, 82]. Preferred candidates for choked-jet SNe are Type Ic SNe [83]. The neutrino emission is expected at the time of the SN explosion and to last $\mathcal{O}(10\,\mathrm{s})$, comparable to the typical GRB duration.

Other models predict neutrino emission from SNe exploding in a dense circum-stellar medium (CSM) [84, 85]. Neutrinos are produced in the interactions of the SNe ejecta with the dense medium on time scales of months.

Supernovae are best discovered in optical wavelength. However, current optical surveys cover only limited regions of the sky or do not go very deep. To overcome this limitation the IceCube collaboration set up an optical follow-up program for interesting neutrino events [86] in 2008. The IceCube data is processed in real-time and the most interesting neutrino events are selected to trigger observations with optical telescopes aiming for the detection of an optical counterpart. The Palomar Transient Factory (PTF) [87] found a Type IIn SN from the direction of a neutrino doublet consisting of two track events which arrived within 1.6 s [88]. However it turned out that the SN was already 160 days old at the time of the neutrino burst and hence is likely a chance coincidence.

5.3. Blazar Flares

In addition to the optical follow-up program IceCube runs a γ-ray follow-up program [89] since March 2012, which triggers the Cherenkov telescopes MAGIC[6] and VERITAS[7]. This program is aiming for the detection of neutrinos in coincidence with γ-ray flares from blazars. A predefined list of known variable γ-ray sources is monitored by IceCube for an excess in neutrinos on time scales of up to three weeks. So far no γ-ray flare was detected in coincidence with a neutrino excess. A hint for neutrino production in blazar flares was claimed in [90], where a PeV neutrino shower event was found in spatial and temporal coincidence with a γ-ray outburst from the blazar PKS B1424-418.

[6] `http:magic.mppmu.mpg.de`

[7] `http://veritas.sao.arizona.edu`

5.4. Public IceCube Alerts

Since beginning of 2016 a real-time event selection for high-energy single track events with high probability of being of astrophysical origin is in place. An expected rate of four high-energy starting track events (HESE) and four extreme high-energy though-going track events (EHE) are selected per year and published in real-time through the Astrophysical Multimessenger Observatory Network (AMON) [91] via the Gamma-Ray Coordinate Network (GCN[8]). The first public neutrino alerts were followed up by various instruments in several wavelengths ranging from optical to γ-ray bands. A detailed overview of the different IceCube real-time channels can be found in [92].

5.5. Gravitational Wave Follow-Up

The detection of the first gravitational wave (GW) event by the advanced LIGO detectors in September 2015 was accompanied by a broad multi-messenger follow-up program aiming for the detection of a counterpart to the GW signal.

IceCube and ANTARES searched their data in a $\pm 500\,\mathrm{s}$ time window centered on the GW event for high-energy neutrinos [93]. No event was detected by ANTARES while IceCube found three events in the time window, which is consistent with background expectations. However those events are not in spatial coincidence with the GW position as shown in Fig. 11. We derive an upper limit on the total energy radiated by neutrinos of 5.4×10^{51} - 1.3×10^{54} erg assuming an energy spectrum following $dN/dE \sim E^{-2}$. Both of the distinct sky regions (see Fig. 11) are considered in the limit calculation to provide an inclusive range.

6. Neutrinos from cosmic-ray interactions in the Galactic plane

Cosmic rays up to a few PeV are believed to originate in Galactic sources. At this energy the CR spectrum shows a break, the so-called CR *knee*, which could indicate that the sources have reached their maximal acceleration energy for the lightest nuclei. It has long been speculated that Galactic core-collapse SNe could be responsible for the observed CR density [94]. These cataclysmic events produce ejecta with kinetic energy of the order of 10^{51} erg per SN explosion at a rate of about three per century. Diffuse shocks that

[8] `http://gcn.gsfc.nasa.gov/`

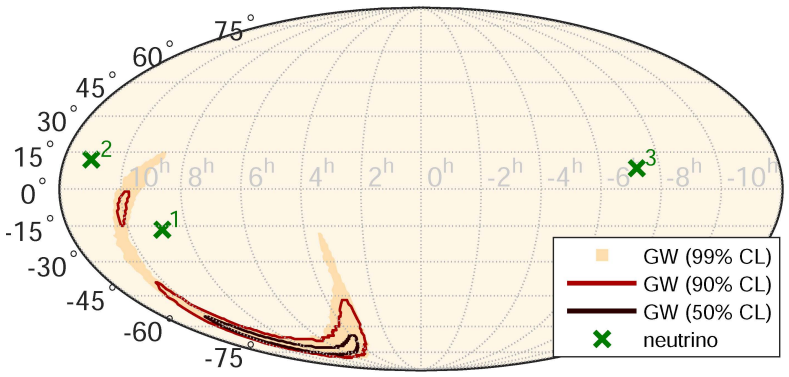

Figure 11: Skymap of the probability density contours of the GW event in equatorial coordinates together with the high-energy neutrino candidates detected by IceCube within a $\pm 500\,\mathrm{s}$ time window centered on the GW event. Figure adopted from Adrian-Martinez et al. [93].

form as the ejecta run into the ambient medium could accelerate particles and could convert a significant fraction of this kinetic energy to a non-thermal population of cosmic rays.

After emission from these sources, CR start to diffuse through Galactic magnetic fields. This process has two effects. First, the arrival directions of CRs become highly isotropized and obscure the position of sources. And, second, the diffusion process softens the spectra compared to the initial emission spectrum due to the enhanced loss of particles at higher energies. Diffusion also implies that the CR density in our Galaxy is rather smooth and can be approximated by the local CR density as $n_{\mathrm{CR}} \simeq 4\pi\phi_{\mathrm{CR}}/c$. This guarantees a diffuse Galactic emission of neutrinos and γ rays from CR interactions with gas in the vicinity of the Galactic Plane [95, 96, 97, 98, 99, 100, 101, 102].

The local emission rate of neutrinos (per flavor) from Galactic CR interactions can be estimated by the local nucleon density n_N as

$$E_\nu^2 Q_\nu(E_\nu) \simeq \frac{1}{6} c n \kappa \sigma_{pp} \left[E_{\mathrm{N}}^2 n_{\mathrm{N}}(E_{\mathrm{N}})\right]_{E_N = 20 E_\nu} \,, \tag{4}$$

where σ_{pp} is the inelastic proton-proton cross section with inelasticity $\kappa \simeq 0.5$ [103, 104]. The factor $1/6$ accounts for the per flavor emission ($\simeq 1/3$), the total neutrino energy fraction in the charge pion decay ($\simeq 3/4$) and for the charged pion fraction in pp collisions ($\simeq 2/3$). The neutrino energy is related to the energy of CR nucleons (N) as $E_\nu \simeq E_N/20$. The target gas density

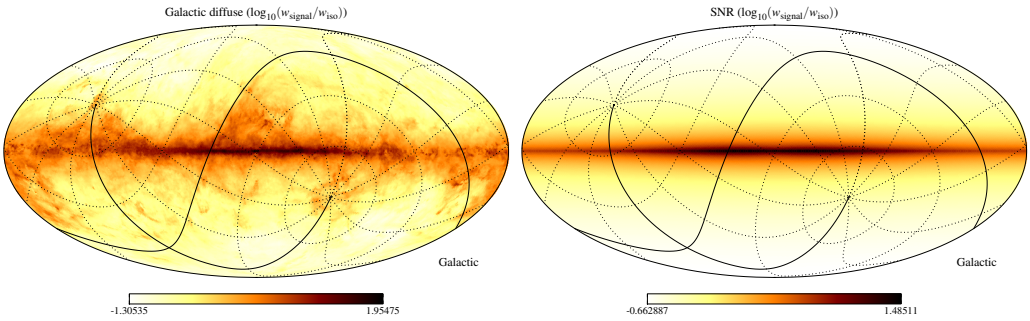

Figure 12: Mollweide projections of diffuse Galactic neutrino emission (from Ref. [102]). The left plot shows diffuse emission from CR propagation ($E_\nu = 10$ TeV) and the right plot the combined emission from supernovae remnants (Case [106]). The mesh indicates the equatorial coordinate system with right ascension $\alpha = 0^\circ$ and declination $\delta = 0^\circ$ indicated as solid lines. The color reflects the logarithm of the intensity ratio between the Galactic and an isotropic signal.

n is mostly concentrated along the Galactic Plane, but can also show high-latitude fluctuations from atomic and molecular gas clouds. The left plot of Fig. 12 shows the predicted intensity of the diffuse emission from Ref. [102] in terms of Galactic coordinates. Note, that the map shows the intensity in logarithmic units. High-latitude intensity fluctuations are generally sub-dominant compared to the Galactic Plane emission.

A simple estimate of the overall diffuse flux around the Galactic Plane can be derived from a simple density scaling $n \simeq \exp(-|z|/0.1\,\mathrm{kpc})$ cm^{-3} with distance z from the Galactic Plane and the corresponding integrated column density along the line-of-sight. The result is shown in Fig. 13 as a red solid line, where we averaged the diffuse emission over latitudes $|b| < 2^\circ$. For the calculation we use Eq. (4) with the locally observed CR nucleon flux derived from the model of Ref. [105]. This estimate agrees well with more elaborate studies using numerical CR propagation codes to evaluate the CR density across the Galaxy and using non-azimuthal target gas maps [102].

Figure 13 shows also the diffuse flux of cosmic neutrinos observed by IceCube [28]. This indicates that the diffuse flux close to the Galactic plane can dominate over the isotropic diffuse emission observed with IceCube for $E_\nu \leq 10$ TeV. However, it is thus unlikely that this Galactic contribution has a strong impact on the interpretation of the IceCube data [107, 108, 109, 102].

Note, that the previous estimate is based on the assumption that we can approximate the average Galactic CR density by the local CR flux. This is not necessarily the case in more general scenarios introducing spatial density fluctuation, e.g., by accounting for anisotropic diffusion [110], by inhomogeneous diffusion [101], or by strongly inhomogeneous source distributions [111, 112]. Alternatively, a time-dependent local CR injection episode could be responsible for local CR spectra that are softer than the Galactic average [113] and could also lead to an increase of the overall Galactic diffuse emission.

The simplest test of Galactic diffuse emission in the IceCube data is by checking for spatial correlations with the Galactic Plane. The 4-year high-energy starting event (HESE) analysis found no significant correlation of events with the Galactic plane. When letting the Galactic Plane size float freely, the best fit returned a value of $|b| \leq 7.5^\circ$ with a post-trial chance probability of 3.3%. The recent analysis [102] based on the 3-year HESE data [21] showed that even with the poor angular resolution of cascade events the anisotropy produced by a strong Galactic diffuse flux should be visible in data. The contribution to the high-energy data with deposited energy above 60 TeV is limited to about 50%. This is in contrast to the claim of Ref. [114] that the 4-year HESE update shows evidence of Galactic emission within latitudes $|b| \leq 10^\circ$ above 100 TeV. However, the angular distribution of the muon neutrino data from the recent analysis [26] does not seem to support this claim. At present, there are various dedicated IceCube analyses that are searching for Galactic diffuse neutrino emission, accounting for uncertainties of morphology and emission spectrum.

Another source of extended Galactic neutrino emission is the cumulative contribution of Galactic sub-threshold sources [115]. While individual Galactic neutrino sources have not been identified, this emission would consists of sources that are below IceCube's detection threshold, but could be identified as extended emission concentrated along the Galactic Plane. If $N_{\rm N}$ is the (time-integrated) CR nucleon spectrum of a single source, we can define the Galactic neutrino emission from interactions of CR with ambient gas as

$$E_\nu^2 Q_\nu(E_\nu) \simeq \frac{1}{6} c n \kappa \sigma_{pp} \rho_{\rm act} \left[E_N^2 N_{\rm N}(E_N)\right]_{E_N=20E_\nu} \,, \tag{5}$$

where n is the ambient gas density and $\rho_{\rm act}$ is the number density of *active* sources in the Galaxy. In the following, we consider the case of neutrino emission from SNRs in our Milky Way [106]. Similar to the diffuse emission

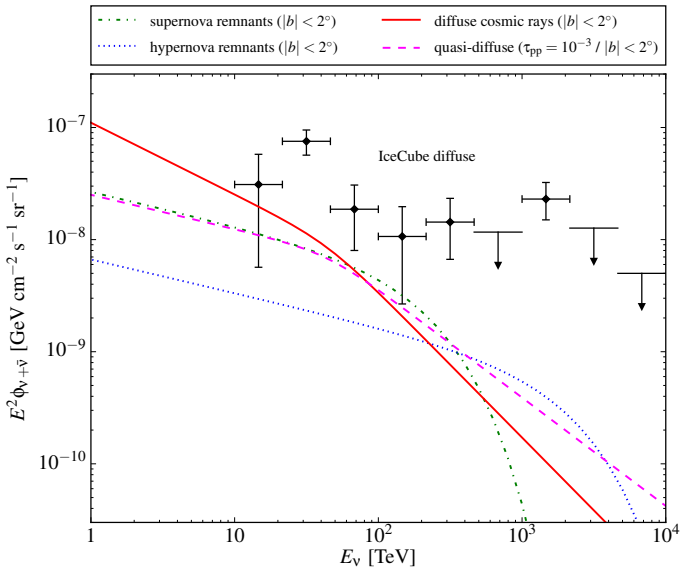

Figure 13: Diffuse emission from the Galactic Plane ($|b| \leq 2°$) in comparison to the isotropic diffuse neutrino flux (per flavor) observed by IceCube [28]. We show the contribution of the Galactic diffuse flux of Eq. (4), the quasi-diffuse flux from Galactic subthreshold sources with optical thickness $\tau_{\rm pp} \simeq 10^{-3}$ and diffuse index $\delta = 1/3$ of in Eq. (6), and the Galactic contribution of supernovae and hypernovae with $\Gamma = 2.3$ in Eq. (5).

from CR propagation, the intensity distribution of events is concentrated along the Galactic Plane as shown in the right plot of Fig. 12.

The number of active SNRs can be estimated from the SN rate and the time-scale of the onset of the snow-plow phase which marks the end of the radiative Sedov phase [116]. From this one can estimate that about one thousand SNRs are CR emitters at any given time. The maximal energy can be estimated from the ambient gas density, ejecta mass, and velocity to reach $E_{\rm max,p} \simeq 5$PeV. Energetic supenovae, so-called *hypernovae*, with ejecta energy $\simeq 10^{52}$ erg and corresponding higher ejecta velocities may reach neutrino energies that are 10 times larger, but they are less frequent than normal supernovae with only 1% - 2% of the supernovae rate [117, 107].

Figure 13 shows the estimated flux of supernova remnants (green dashed-dotted line) and hypernova remnants (blue dotted line) following the lines of arguments of Ref. [107] with a source spectral index $\Gamma \simeq 2.3$. Since the source emission spectrum is much harder than the diffuse CR spectrum the flux is expected to become more important at higher energies, corresponding

to neutrino production of CRs close to the knee region.

Note, that the previous estimate does not depend on the question if SNR are the main sources of Galactic CRs. If we focus on the sources of Galactic CRs, we can relate the (per flavor) neutrino emission rate to that of the CR nucleons as

$$E_\nu^2 Q_\nu(E_\nu) \simeq \frac{1}{6}\kappa\tau_{pp}\left[E_N^2 Q_{\rm N}(E_N)\right]_{E_N=20E_\nu} \ , \tag{6}$$

where $\tau_{pp} \ll 1$ is the optical thickness of the source environment for CR-gas interactions, before CRs are released into the Galactic medium. The nucleon emission rate $Q_{\rm N}$ is now fixed to the observed CR spectrum by the steady-state solution of the CR diffusion equation. For a source emitting during a time-scale $t_{\rm act}$ and average gas density $n_{\rm gas}$ the optical thickness is given as $\tau_{pp} \simeq ct_{\rm act}n_{\rm gas}\sigma_{pp}$. For instance, in the case of SNR we can estimate $t_{\rm act}$ by dynamical time-scale as 10^4 yr, the beginning of the snowplow phase [116], and $n_{\rm gas} \simeq 1{\rm cm}^{-3}$ yielding $\tau_{pp} \simeq 3\times10^{-4}$. The flux is shown in Fig. 13 as a magenta dashed line assuming $\tau_{\rm pp} \simeq 10^{-3}$ and diffusion index $\delta = 1/3$. Not surprisingly, this is consistent with our previous estimates of the combined flux of supernova and hypernova remnants.

Similar to the case of the diffuse Galactic emission, the contribution of weak Galactic sources are constrained by the absence of anisotropies. In Ref. [102] it was shown that candidate Galactic sources for the IceCube emission following the Galactic distribution of supernova remnants [107, 118] or pulsars [119, 120] can not contribute more than 65% to be consistent with the HESE three-year data [102].

7. Measurements of the local cosmic-ray spectrum and composition

From the point of view of cosmic-ray physics, IceCube is a three-dimensional air shower array. The aperture for trajectories that pass through IceTop and within the deep array at its mid-plane is ≈ 0.25 km^{2}sr, which corresponds to ≈ 1000 events per year above 100 PeV, but ≤ 1 event per year above one EeV. Such coincident events provide information about primary composition from the ratio of the energy in the muon bundle in the deep ice to the total shower size at the surface. The measurement of the primary spectrum can be extended to the PeV range by using events over a larger angular range reconstructed with the surface array only [121]. Muon bundles reconstructed over a large range of zenith angles with the deep array of IceCube extend

the acceptance into the EeV range and provide complementary information to the surface array [122]. IceCube can resolve muons laterally separated from the main core in the deep array by more than the string spacing. The separation distribution measured out to 400 meters shows the concave shape expected from the transition from exponential to power-law for the transverse momentum distribution of the parent mesons [123].

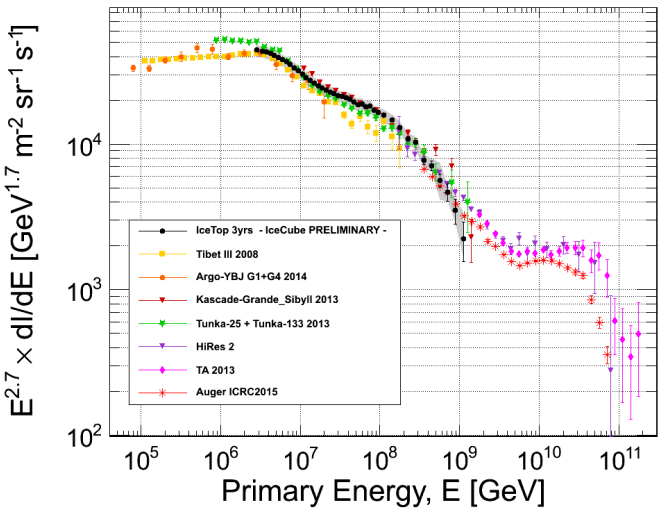

Figure 14: A summary of the primary spectrum from selected air shower experiments. Measurement from three years of data in IceCube [124] are shown by the black squares.

Several aspects of IceTop lead to its good energy resolution and its ability to distinguish features in the energy spectrum. The array is at a high altitude so that events are observed closer to shower maximum. As a consequence, fluctuations from event to event are less severe than in an array near sea level. The ice Cherenkov tanks are approximately two radiation lengths deep so that the dominant photon component of the surface shower is counted as well as the charged leptons. In contrast, most photons pass through scintillators without converting. The IceTop results are shown by the black points in the compilation of air-shower data in Fig. 14. In addition to the knee above 3 PeV, there is a significant hardening of the spectrum around 20 PeV, and the second knee is visible above 200 PeV.

IceCube is the only air shower array currently in operation that can detect TeV muons in the shower core in coincidence with the main shower at the

surface. It has much larger acceptance than its predecessors, EASTOP-MACRO [125] and SPASE-AMANDA [126]. Preliminary analysis of the coincidence data in IceCube shows the composition becoming increasingly heavy through the knee region to 100 PeV and beyond [124], although the results become statistically limited at the highest energies.

The increasing fraction of heavy primaries is expected if the knee is the result of Galactic CR accelerators reaching their upper limit. Air shower experiments make calorimetric measurements of the total energy per particle. Since acceleration and propagation of CR are both determined by magnetic fields, features in the spectrum should instead depend on magnetic rigidity [127]. Thus, for example, if the characteristic maximum energy for protons is 4 PeV, there should be a corresponding steepening for iron nuclei around 100 PeV total energy. Several air-shower measurements, as reviewed in [128], show the composition changing back toward a lighter composition above 100 PeV as might be expected with the onset of an extra-galactic component at higher energy. The IceCube coincidence analysis give composition results that agree well with $\langle \ln(A) \rangle$ summary of Ref. [128] up to 100 PeV, but the mass value remains high above that energy, in some tension with the other data. (See Fig. 8 in [129].)

Muons produce a characteristic signal in IceTop tanks because they generate a charge proportional to the length of their tracks. In addition, as the main electromagnetic part of the signal falls off at large distance from the shower core, muons become increasingly prominent, as indicated by the "thumb" centered near one Vertical Equivalent Muon (VEM) in Fig. 15. This leads to the possibility of measuring the contribution of $\sim$ GeV muons to the showers at the surface [130]. Such a measure of the fraction of muons at the surface opens the possibility of a different quantity that is sensitive to primary composition. Information from the low energy muons at the surface is complementary to the TeV muons in the shower cores in the coincident event analysis. The comparison, which is ongoing, is of particular interest in light of the fact that different hadronic interaction models show a different behavior for the ratio of GeV to TeV muons. In addition, there are indications that all the standard event generators for >EeV air showers produce fewer muons at the surface than observed [131].

Because muons are rare in cascades initiated by photons, the muon content can also be used to reduce the CR background in a search for $\sim$ PeV γ-rays. A shower reconstructed at the surface with a trajectory that passes through the deep array of IceCube without leaving a signal is a γ-ray can-

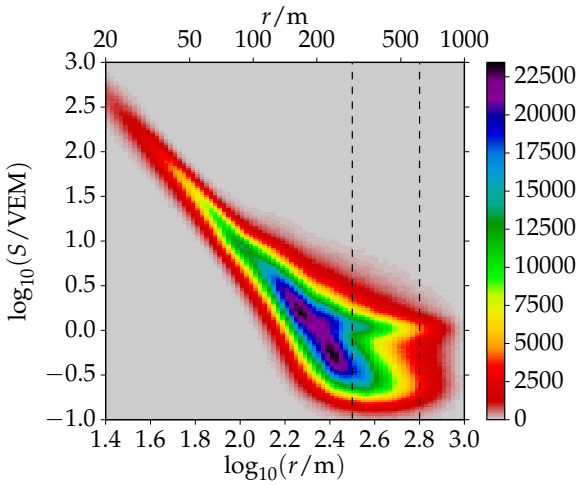

Figure 15: Two-dimensional distribution of signals in showers with primary energies of *approx*3 PeV and zenith angles around 13° as a function of signal in VEM and reconstructed core distance. The horizontal dashed lines indicate the distances at which muon densities as a function of primary energy have been reported [130].

didate. Because of energy losses in the CMB, only Galactic sources would be visible in PeV photons. Using one year of data taken when IceCube was partially complete with 40 strings, a limit on γ rays of several PeV from the Galactic plane was set [132]. Because of the small zenith angle required for events to pass through both components of IceCube, the search was limited to Southern declinations $< -60°$. Therefore the analysis covers a limited region of the Galactic plane, $-80° < \ell < -30°$ in longitude and $-10° < b < 5°$ in latitude. The sensitivity with five years of data from the full IceCube detector is estimated to be comparable to expectations from some known TeV γ-ray sources in this region if their spectra continue to a PeV without steepening. An analysis with the completed IceCube detector is underway. Including muon information from the surface detector will allow a larger region of the sky to be explored.

Another search for Galactic CR sources looks for neutrons [133], which would show up as point sources of air showers above the the smooth background of charged CR. No such excesses are identified in 4 years of IceTop data. Limits are placed on potential accelerators of CR protons and nuclei, including millisecond pulsars and high mass x-ray binaries, by using events

with energy > 100 PeV for which the mean distance a neutron would travel before decaying is 100 kpc. Assuming an E^{-2} spectrum, the limits are of the same order of magnitude in energy flux as what might be expected for sources that produce photons in association with acceleration of nuclei that fragment in or near their sources to produce neutrons.

8. Anisotropy of local cosmic rays

Through measurement of the energy spectrum and composition of the cosmic-ray flux, we hope to gain a better understanding of CR sources and acceleration mechanisms. Another quantity accessible to experimental measurement is the arrival direction of the CR particles. In principle, the sky map of CR arrival directions should give us the most direct indication of where the sources might be located. Below several PeV, the sources of CR are Galactic and the arrival direction distribution should show a correlation with the Galactic plane. However, unlike γ rays and neutrinos, CR particles are charged and therefore repeatedly scattered in chaotic magnetic fields. Their arrival direction distribution on Earth is highly isotropic, although a small residual dipole anisotropy is expected from diffusion theory.

Observations made over the last few decades with various surface and underground detectors, together covering an energy range from tens of GeV to tens of PeV, have indeed provided statistically significant evidence for a faint anisotropy in the CR arrival direction distribution [10, 11, 12, 13, 14, 15, 134, 135, 136, 137, 138]. The anisotropy is small, with an amplitude on the order of 10^{-3}, and it shows a strong dependence on energy [139, 140, 138]. It is, however, not well described by a simple dipole. A quantitative description of the anisotropy as a superposition of spherical harmonics [138, 141] shows that while most of the power is in the low-multipole ($\ell \leq 4$) terms, i.e., in the dipole, quadrupole, and octupole terms, features with smaller angular scale down to sizes of a few degrees are also present. These small-scale features have been observed in the TeV range by several experiments [142, 143, 136, 134, 141, 138], and their relative intensity is on the order of 10^{-5}–10^{-4}. Given the complex nature of the anisotropy, its range from large to small angular scales, and its strong dependence on energy, it has become clear that there is no single process that can account for all observations. Rather, multiple phenomena likely contribute to the anisotropy.

Before IceCube, high-statistics measurements of the CR anisotropy in the TeV to PeV energy range were only available from experiments in the

Northern Hemisphere. Over the last few years, IceCube has accumulated one of the largest CR data sets, and a detailed study of the morphology, energy dependence, and stability of the anisotropy over time is possible for the southern sky.

CR can be studied with IceCube in two independent ways. The in-ice component of IceCube detects downward-going muons created in extensive air showers caused by CR entering the atmosphere above the detector. Simulations show that the detected muon events are generated by primary CR particles with median energy of about 20 TeV. The trigger rate ranges between 2 and 2.4 kHz, with the modulation caused by seasonal variations of the stratospheric temperature and density.

The anisotropy can also be studied using the CR air showers detected by IceTop. Its surface location near the shower maximum makes it sensitive to the full electromagnetic component of the shower, not just the muonic component. The detection rate is approximately 30 Hz and the minimum primary particle energy threshold is about 400 TeV. Requiring a minimum of eight IceTop stations leads to a median energy of 1.6 PeV. The IceTop data set therefore provides an independent measurement at PeV energies, close to the knee of the CR spectrum.

A recent study of the CR anisotropy in IceCube and IceTop [138] is based on six years of data taken between May 2009 and May 2015. The data set contains 318 billion CR events observed by IceCube and 172 million events observed with IceTop at higher energies. In order to study the energy dependence of the anisotropy, the IceCube data set is split into nine bins of increasing median energy, ranging from TeV to PeV. The resolution of this energy assignment depends on the detector configuration and energy band but is on the order of 0.5 in $\log_{10}(E/\mathrm{GeV})$. It is primarily limited by the relatively large fluctuations in the fraction of the total shower energy that is transferred to the muon bundle.

The most prominent anisotropy observed in the IceCube maps at energies below 50 TeV is characterized by a large excess from 30° to 120° in right ascension and a deficit from 150° to 250°. The relative intensity of the anisotropy is at the 10^{-3} level. This large-scale structure that dominates the sky map at lower energies gradually disappears above 50 TeV. Above 100 TeV, a change in the morphology is observed. At higher energies, the anisotropy is characterized by a wide relative deficit from 30° to 120°, with an amplitude increasing with energy up to at least 5 PeV, the highest energies currently accessible to IceCube. The IceTop map at 1.6 PeV shows the same

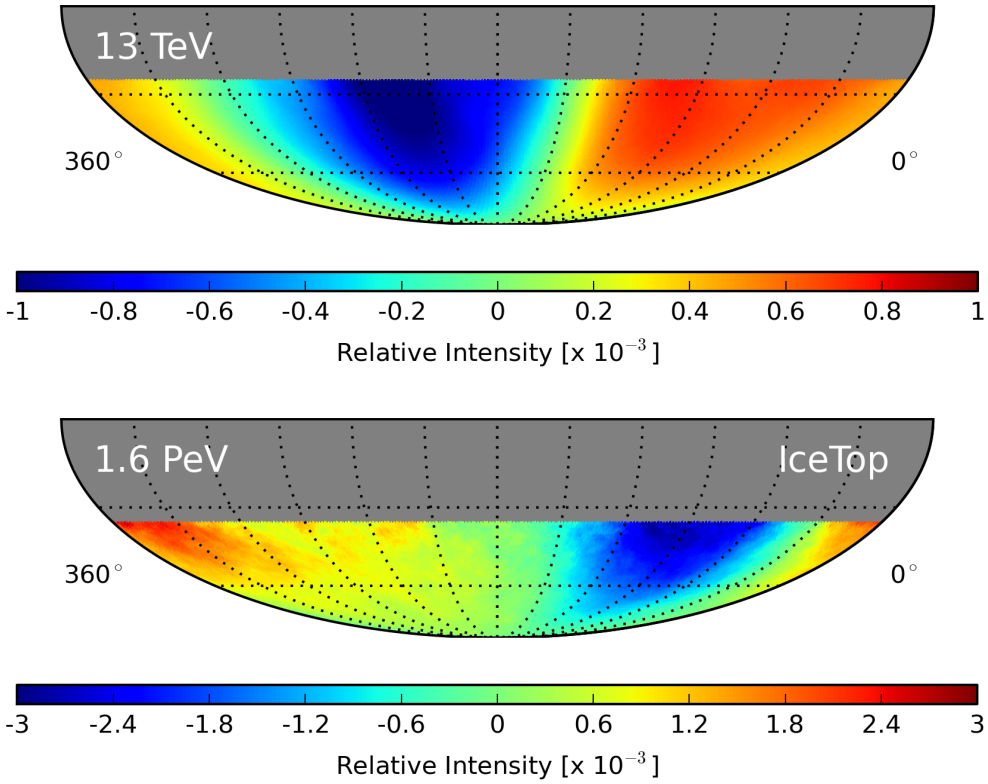

Figure 16: Relative intensity maps in equatorial coordinates for a median energy of 13 TeV (top) and 1.6 PeV (bottom). The low-energy map is based on IceCube data, the high-energy map on IceTop data. Maps have been smoothed with a 20° smoothing radius.

morphology as the IceCube maps at comparable energies. To illustrate this change of the phase of the large-scale anisotropy between TeV and PeV energies, Fig. 16 shows the IceCube map at a median energy of 13 TeV (top) to the IceTop map at 1.6 PeV (bottom).

Fig. 17 shows the phase (top) and amplitude (bottom) of the dipole component as a function of energy. Since the data is not well described by a dipole, the actual fit is performed including higher-order multipoles, but only the amplitude and phase of the dipole are reported here. The phase shift in the dipole component of the large-scale anisotropy occurs rather rapidly between 100 TeV and 200 TeV. The amplitude of the dipole component rises with energy up to about 10 TeV. Above this energy, it slowly decreases until

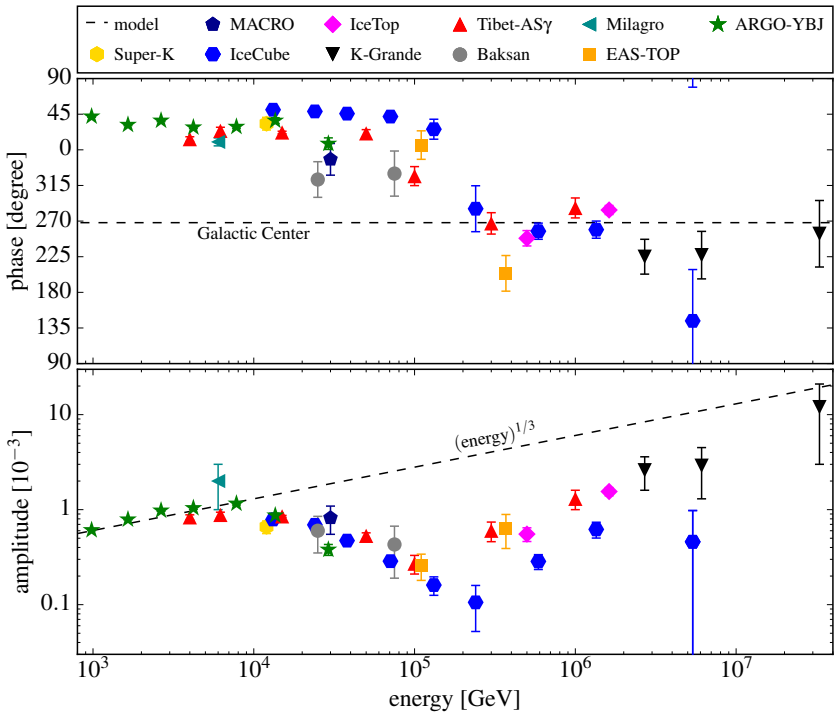

Figure 17: Phase (top) and amplitude (bottom) of the dipole moment of the CR relative intensity map as a function of energy for IceCube (blue), IceTop (pink), and other experiments. Taken from [144].

it has essentially dropped by an order of magnitude at around 200 TeV. It then increases again, with a different phase, up to the highest detected energies. The figure also shows the results from several other experiments in the Northern Hemisphere. The results are generally in good agreement. The difference in the amplitude measured by IceCube and IceTop above 1 PeV is likely due to a difference in the chemical composition of the two data sets. At this energy, the IceTop data set has on average a lighter composition than the IceCube data set because IceTop is not yet fully sensitive to heavier nuclei.

Measurements of a dipole amplitude and phase of the CR flux have also been performed at even higher energies, although the small rate makes these measurements increasingly difficult. Nevertheless, the Pierre Auger Observatory found that a shift in the phase of the anisotropy occurs again at EeV energies [145]. Below 1 EeV, the dipole phase is consistent with the phase observed by IceCube at PeV energies. Around 4 EeV, the phase changes and

the relative excess moves towards the range in right ascension that includes the Galactic anti-center direction. In between the IceCube and Pierre Auger measurements, KASCADE-Grande data shows a dipole phase between median energies of 2.7 PeV and 33 PeV, which is consistent with the IceCube results at PeV energies [146].

While the large-scale structure dominates the anisotropy, there is also anisotropy on smaller scales. The small-scale structure, with a relative intensity on the order of 10^{-4} and therefore roughly one order of magnitude weaker, becomes visible after the best-fit dipole and quadrupole are subtracted from the sky map. Fig. 18 shows the relative intensity of the residual map. Several excess and deficit regions are visible at angular scales approaching the angular resolution of IceCube for CR primaries. The strongest of these regions have statistical significances exceeding $10\,\sigma$.

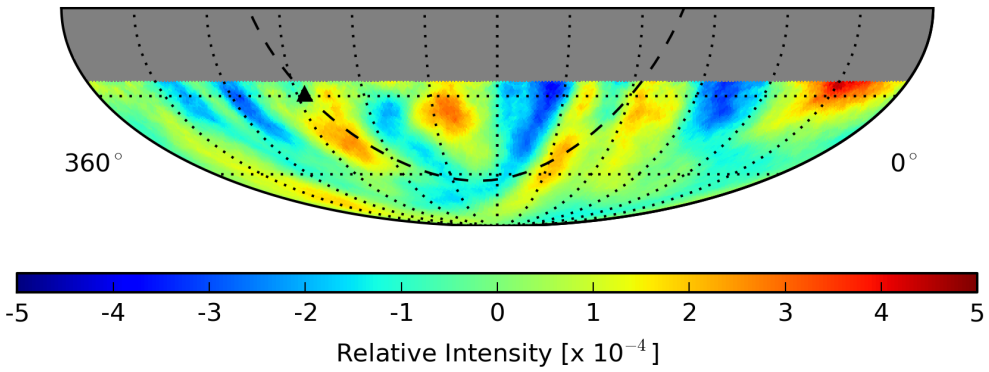

Figure 18: Relative intensity map of the full 6-year IceCube data set for all energies (median energy 20 TeV) after dipole- and quadrupole-subtraction. The subtraction of the dominant low-order multipoles reveals the small-scale structure, with a relative intensity of order 10^{-4}. The dashed line indicates the Galactic plane and the triangle indicates the Galactic center.

A study of the time dependence of the large- and small-scale structure over the six-year period covered by this analysis reveals no significant change with time. An analysis of data taken with the AMANDA detector between 2000 and 2006 also did not find any significant time variation of the observed anisotropy [147].

The source of the CR anisotropy remains unknown. The large-scale anisotropy can be qualitatively explained by homogeneous and isotropic diffusive propagation of CR in the Galaxy from stochastically distributed sources.

Several authors have shown that particular realizations of Galactic source distributions reproduce the observed energy dependence. The phase shift between TeV and PeV energies could indicate that the location of the dominant source(s) shifts. Below 100 TeV, the phase coincides with the direction of the Orion arm, whereas the phase above the shift coincides with the right ascension of the Galactic center, $\alpha_{GC} = 268.4°$. As a caveat, simulations based on plausible source distributions typically predict a larger amplitude for the anisotropy than what is observed [148, 149, 150, 151, 152].

Recently, it has been shown that one or more local sources at Galactic longitude between 120° and 300° and the presence of a strong ordered magnetic field in our local environment can explain the observations [153]. The Vela supernova remnant, created about 12,000 years ago, is identified as a candidate. The discrepancy between the predicted and observed amplitude could, at least in part, be a result of the limited capabilities of ground-based detectors to reconstruct the true underlying anisotropy.

The small-scale anisotropy may be produced by the interactions of CR with an isotropically turbulent interstellar magnetic field. Scattering processes with stochastic magnetic instabilities produce perturbations in the arrival direction distribution of an anisotropic distribution of CR particles within the scattering mean free path. Such perturbations may be observed as stochastic localized excess or deficit regions [154, 155, 156, 157].

There are other sources of magnetic perturbations on smaller scales, for example the heliosphere, formed by the interaction between the solar wind and the interstellar flow. The heliosphere constitutes a perturbation in the 3 μG local interstellar magnetic field. The local magnetic field draping around the heliosphere might be a significant source of resonant scattering, capable of redistributing the arrival directions of TeV CR particles.

9. Conclusions

We have reviewed how observations of neutrinos and cosmic rays with the IceCube neutrino telescope and its surface array IceTop have impacted our knowledge about the high-energy non-thermal universe. Only three years after their first detection, we know the spectrum and flavor composition of cosmic neutrinos in the energy interval between 10 TeV and several PeV with encouraging precision. The distribution of the neutrinos on the sky is compatible with an isotropic distribution, excluding a purely Galactic origin.

Surprisingly, no individual neutrino sources or transients were observed so far that would pinpoint the origin of the cosmic neutrinos. However, putting all the information together, we can already make important statements about their origin. Blazar jets and Gamma-ray bursts can only be responsible for small fractions of the observed cosmic neutrinos. Less luminous sources with higher number densities are needed to explain the observed level of astrophysical neutrinos, and the absence of detectable point sources at the same time. Interesting coincidences of neutrino events with transient pheonomena, a supernova explosion and a Blazar flare, have been seen, however the circumstances make it impossible to exclude a chance coincidence.

No neutrinos have been observed that could be attributed to the GZK effect, the production of neutrinos from interactions of UHECR during their propagation in the intergalactic radiation fields. Also here the non-observation of associated neutrinos starts to constrain evolution scenarios for UHECR sources.

Direct observations of spectrum and anisotropy of CR at TeV and PeV energies with IceCube and IceTop have provided an accurate measurements of the shape of the CR spectrum from few PeV to above one EeV. Searches for point sources of photons or neutrons among the CR air showers recorded have been negative so far. Addionally, the large statistics of CR air showers has allowed the most precise measurement of the CR anisotropy in the Southern hemisphere, confirming and extending measurements on the Northern hemisphere. Both large-scale and small-scale components are detected, however their origin is still not well understood.

Both IceCube and IceTop continue to collect data, likely for at least another decade. As the statistics of cosmic neutrinos and CR increases and the understanding of systematic effects improves, we can expect significant advances in understanding the neutrino sky, the origin of CR, and their propagation and arrival at Earth.

However, there are also limitations to what IceCube can achieve by collecting more statistics. Based on the experience and success of IceCube, current efforts are therefore underway towards a next generation instrument, IceCube-Gen2 [158]. With its five times better sensitivity for sources than IceCube, ten times the statistics for cosmic neutrinos and at least ten times larger area for a surface array, it will truly mark the next big step towards understanding the origin and propagation of cosmic rays.

[1] M. G. Aartsen, et al., Evidence for High-Energy Extraterrestrial Neutrinos at the IceCube Detector, Science 342 (2013) 1242856.

[2] A. M. Hillas, The Origin of Ultra-High-Energy Cosmic Rays, Annual review of astronomy and astrophysics 22 (1984) 425–444.

[3] E. Waxman, J. N. Bahcall, High-energy neutrinos from cosmological gamma-ray burst fireballs, Phys. Rev. Lett. 78 (1997) 2292–2295.

[4] K. Fang, K. Kotera, A. V. Olinto, Newly-born pulsars as sources of ultrahigh energy cosmic rays, Astrophys. J. 750 (2012) 118.

[5] K. Mannheim, The proton blazar, Astronomy and Astrophysics 269 (1993) 67–76.

[6] F. W. Stecker, C. Done, M. H. Salamon, P. Sommers, High-energy neutrinos from active galactic nuclei, Physical Review Letters 66 (1991) 2697–2700.

[7] K. Kashiyama, P. Mészáros, Galaxy Mergers as a Source of Cosmic Rays, Neutrinos, and Gamma Rays, Astrophys. J. Lett. 790 (2014) L14.

[8] M. Ahlers, et al. (2010). FERMILAB-FN-0847-A, YITP-SB-10-01.

[9] K. A. Olive, Review of Particle Physics, Chin. Phys. C40 (2016) 100001.

[10] M. Amenomori, et al., Large-Scale Sidereal Anisotropy of Galactic Cosmic-Ray Intensity Observed by the Tibet Air Shower Array, Astrophys. J. Lett. 626 (2005) L29–L32.

[11] M. Amenomori, et al., Anisotropy and Corotation of Galactic Cosmic Rays, Science 314 (2006) 439–443.

[12] G. Guillian, et al., Observation of the anisotropy of 10TeV primary cosmic ray nuclei flux with the Super-Kamiokande-I detector, Phys. Rev. D 75 (2007) 062003.

[13] A. Abdo, et al., The Large-Scale Cosmic-Ray Anisotropy as Observed with Milagro, Astrophys. J. 698 (2009) 2121–2130.

[14] J. De Jong, et al., Observations of Large Scale Sidereal Anisotropy in 1 and 11 TeV cosmic rays from the MINOS experiment., Proc. 32nd Int. Cosmic Ray Conference, Beijing, China 4 (2011) 46.

[15] B. Bartoli, et al., Argo-ybj observation of the large-scale cosmic ray anisotropy during the solar minimum between cycles 23 and 24, Astrophys. J. 809 (2015) 90.

[16] S. Adrian-Martinez, et al., Letter of intent for KM3NeT 2.0, J. Phys. G43 (2016) 084001.

[17] A. D. Avrorin, et al., Sensitivity of the Baikal-GVD neutrino telescope to neutrino emission toward the center of the galactic dark matter halo, JETP Lett. 101 (2015) 289–294.

[18] M. G. Aartsen, et al., Energy reconstruction methods in the IceCube neutrino telescope, Journal of Instrumentation 9 (2014) P03009.

[19] R. Abbasi, et al., IceTop: The surface component of IceCube, Nucl. Instrum. Meth. A700 (2013) 188–220.

[20] M. G. Aartsen, et al., First observation of PeV-energy neutrinos with IceCube, Phys. Rev. Lett. 111 (2013) 021103.

[21] M. G. Aartsen, et al., Observation of High-Energy Astrophysical Neutrinos in Three Years of IceCube Data, Phys. Rev. Lett. 113 (2014) 101101.

[22] M. G. Aartsen, et al., The IceCube Neutrino Observatory - Contributions to ICRC 2015 Part II: Atmospheric and Astrophysical Diffuse Neutrino Searches of All Flavors, 6: Observation of Astrophysical Neutrinos in four Years of IceCube Data, in: Proceedings, 34th International Cosmic Ray Conference (ICRC 2015): The Hague, The Netherlands, July 30-August 6, 2015.

[23] M. G. Aartsen, et al., Atmospheric and astrophysical neutrinos above 1 TeV interacting in IceCube, Phys. Rev. D91 (2015) 022001.

[24] M. G. Aartsen, et al., The IceCube Neutrino Observatory - Contributions to ICRC 2015 Part II: Atmospheric and Astrophysical Diffuse

Neutrino Searches of All Flavors, 9: High Energy Astrophysical Neutrino Flux Characteristics for Neutrino-induced Cascades Using IC79 and IC86-String IceCube Configurations, in: Proceedings, 34th International Cosmic Ray Conference (ICRC 2015): The Hague, The Netherlands, July 30-August 6, 2015.

[25] M. G. Aartsen, et al., Evidence for Astrophysical Muon Neutrinos from the Northern Sky with IceCube, Phys. Rev. Lett. 115 (2015) 081102.

[26] M. G. Aartsen, et al., Observation and Characterization of a Cosmic Muon Neutrino Flux from the Northern Hemisphere using six years of IceCube data (2016).

[27] M. G. Aartsen, et al., Search for Astrophysical Tau Neutrinos in Three Years of IceCube Data, Phys. Rev. D93 (2016) 022001.

[28] M. G. Aartsen, et al., A combined maximum-likelihood analysis of the high-energy astrophysical neutrino flux measured with IceCube, Astrophys. J. 809 (2015) 98.

[29] M. G. Aartsen, et al., All-sky search for time-integrated neutrino emission from astrophysical sources with 7 years of IceCube data (2016).

[30] S. Adrian-Martinez, et al., Searches for Point-like and extended neutrino sources close to the Galactic Centre using the ANTARES neutrino Telescope, Astrophys. J. 786 (2014) L5.

[31] A. Reimer, Photon-neutrino flux correlations from hadronic models of AGN?, Proceedings, 34th International Cosmic Ray Conference (ICRC 2015) (2015).

[32] M. Petropoulou, S. Dimitrakoudis, P. Padovani, A. Mastichiadis, E. Resconi, Photohadronic origin of γ -ray BL Lac emission: implications for IceCube neutrinos, MNRAS 448 (2015) 2412–2429.

[33] M. G. Aartsen, et al., Search for Time-independent Neutrino Emission from Astrophysical Sources with 3 yr of IceCube Data, Astrophys. J. 779 (2013) 132.

[34] M. G. Aartsen, et al., Searches for Extended and Point-like Neutrino Sources with Four Years of IceCube Data, Astrophys. J. 796 (2014) 109.

[35] R. Abbasi, et al., Time-Dependent Searches for Point Sources of Neutrinos with the 40-String and 22-String Configurations of IceCube, Astrophys. J. 744 (2012) 1.

[36] S. Adrian-Martinez, et al., Search for Cosmic Neutrino Point Sources with Four Year Data of the ANTARES Telescope, Astrophys. J. 760 (2012) 53.

[37] R. Abbasi, et al., An absence of neutrinos associated with cosmic-ray acceleration in γ-ray bursts, Nature 484 (2012) 351–353.

[38] S. Adrian-Martinez, et al., Search for muon neutrinos from gamma-ray bursts with the ANTARES neutrino telescope using 2008 to 2011 data, Astron. Astrophys. 559 (2013) A9.

[39] M. G. Aartsen, et al., Searches for Time Dependent Neutrino Sources with IceCube Data from 2008 to 2012, Astrophys. J. 807 (2015) 46.

[40] P. Lipari, Perspectives of High Energy Neutrino Astronomy, Nucl. Instrum. Meth. A567 (2006) 405–417.

[41] J. K. Becker, W. Rhode, P. L. Biermann, K. Muenich, Astrophysical implications of high energy neutrino limits. 1. Overall diffuse limits, Astropart. Phys. 28 (2008) 98–118.

[42] A. Silvestri, S. W. Barwick, Constraints on Extragalactic Point Source Flux from Diffuse Neutrino Limits, Phys.Rev. D81 (2010) 023001.

[43] M. Ahlers, F. Halzen, Pinpointing Extragalactic Neutrino Sources in Light of Recent IceCube Observations, Phys. Rev. D90 (2014) 043005.

[44] A. M. Hopkins, J. F. Beacom, On the normalisation of the cosmic star formation history, Astrophys. J. 651 (2006) 142–154.

[45] H. Yuksel, M. D. Kistler, J. F. Beacom, A. M. Hopkins, Revealing the High-Redshift Star Formation Rate with Gamma-Ray Bursts, Astrophys. J. 683 (2008) L5–L8.

[46] T. Glüsenkamp, Analysis of the cumulative neutrino flux from Fermi-LAT blazar populations using 3 years of IceCube data, EPJ Web Conf. 121 (2016) 05006.

[47] K. Greisen, End to the cosmic ray spectrum?, Phys. Rev. Lett. 16 (1966) 748–750.

[48] G. T. Zatsepin, V. A. Kuzmin, Upper limit of the spectrum of cosmic rays, JETP Lett. 4 (1966) 78–80. [Pisma Zh. Eksp. Teor. Fiz.4,114(1966)].

[49] V. S. Berezinsky, G. T. Zatsepin, Cosmic rays at ultrahigh-energies (neutrino?), Phys. Lett. B28 (1969) 423–424.

[50] S. Yoshida, M. Teshima, Energy spectrum of ultrahigh-energy cosmic rays with extragalactic origin, Prog. Theor. Phys. 89 (1993) 833–845.

[51] R. J. Protheroe, P. A. Johnson, Propagation of ultrahigh-energy protons over cosmological distances and implications for topological defect models, Astropart. Phys. 4 (1996) 253.

[52] R. Engel, D. Seckel, T. Stanev, Neutrinos from propagation of ultrahigh-energy protons, Phys. Rev. D64 (2001) 093010.

[53] V. Berezinsky, A. Z. Gazizov, S. I. Grigorieva, On astrophysical solution to ultrahigh-energy cosmic rays, Phys. Rev. D74 (2006) 043005.

[54] Z. Fodor, S. D. Katz, A. Ringwald, H. Tu, Bounds on the cosmogenic neutrino flux, JCAP 0311 (2003) 015.

[55] H. Yuksel, M. D. Kistler, Enhanced cosmological GRB rates and implications for cosmogenic neutrinos, Phys. Rev. D75 (2007) 083004.

[56] H. Takami, K. Murase, S. Nagataki, K. Sato, Cosmogenic neutrinos as a probe of the transition from Galactic to extragalactic cosmic rays, Astropart. Phys. 31 (2009) 201–211.

[57] V. Berezinsky, A. Gazizov, M. Kachelriess, S. Ostapchenko, Restricting UHECRs and cosmogenic neutrinos with Fermi-LAT, Phys. Lett. B695 (2011) 13–18.

[58] M. Ahlers, L. A. Anchordoqui, M. C. Gonzalez-Garcia, F. Halzen, S. Sarkar, GZK Neutrinos after the Fermi-LAT Diffuse Photon Flux Measurement, Astropart. Phys. 34 (2010) 106–115.

[59] G. B. Gelmini, O. Kalashev, D. V. Semikoz, Gamma-Ray Constraints on Maximum Cosmogenic Neutrino Fluxes and UHECR Source Evolution Models, JCAP 1201 (2012) 044.

[60] G. Decerprit, D. Allard, Constraints on the origin of ultrahigh energy cosmic rays from cosmogenic neutrinos and photons, Astron. Astrophys. 535 (2011) A66.

[61] J. Heinze, D. Boncioli, M. Bustamante, W. Winter, Cosmogenic Neutrinos Challenge the Cosmic Ray Proton Dip Model, Astrophys. J. 825 (2016) 122.

[62] A. Supanitsky, Implications of gamma-ray observations on proton models of ultrahigh energy cosmic rays, Phys. Rev. D94 (2016) 063002.

[63] A. A. Abdo, et al., The Spectrum of the Isotropic Diffuse Gamma-Ray Emission Derived From First-Year Fermi Large Area Telescope Data, Phys. Rev. Lett. 104 (2010) 101101.

[64] M. Ackermann, et al., The spectrum of isotropic diffuse gamma-ray emission between 100 MeV and 820 GeV, Astrophys. J. 799 (2015) 86.

[65] D. Hooper, A. Taylor, S. Sarkar, The Impact of heavy nuclei on the cosmogenic neutrino flux, Astropart. Phys. 23 (2005) 11–17.

[66] M. Ave, N. Busca, A. V. Olinto, A. A. Watson, T. Yamamoto, Cosmogenic neutrinos from ultra-high energy nuclei, Astropart. Phys. 23 (2005) 19–29.

[67] D. Hooper, S. Sarkar, A. M. Taylor, The intergalactic propagation of ultrahigh energy cosmic ray nuclei, Astropart. Phys. 27 (2007) 199–212.

[68] D. Allard, et al., Cosmogenic Neutrinos from the propagation of Ultrahigh Energy Nuclei, JCAP 0609 (2006) 005.

[69] L. A. Anchordoqui, H. Goldberg, D. Hooper, S. Sarkar, A. M. Taylor, Predictions for the Cosmogenic Neutrino Flux in Light of New Data from the Pierre Auger Observatory, Phys. Rev. D76 (2007) 123008.

[70] R. Aloisio, V. Berezinsky, A. Gazizov, Ultra High Energy Cosmic Rays: The disappointing model, Astropart. Phys. 34 (2011) 620–626.

[71] K. Kotera, D. Allard, A. V. Olinto, Cosmogenic Neutrinos: parameter space and detectabilty from PeV to ZeV, JCAP 1010 (2010) 013.

[72] M. Ahlers, J. Salvado, Cosmogenic gamma-rays and the composition of cosmic rays, Phys. Rev. D84 (2011) 085019.

[73] M. Ahlers, F. Halzen, Minimal Cosmogenic Neutrinos, Phys. Rev. D86 (2012) 083010.

[74] M. G. Aartsen, et al., Constraints on ultra-high-energy cosmic ray sources from a search for neutrinos above 10 PeV with IceCube (2016).

[75] M. G. Aartsen, et al., An All-Sky Search for Three Flavors of Neutrinos from Gamma-Ray Bursts with the IceCube Neutrino Observatory, Astrophys. J. 824 (2016) 115.

[76] M. Ahlers, M. C. Gonzalez-Garcia, F. Halzen, GRBs on probation: testing the UHE CR paradigm with IceCube, Astropart. Phys. 35 (2011) 87–94.

[77] M. Bustamante, P. Baerwald, K. Murase, W. Winter, Neutrino and cosmic-ray emission from multiple internal shocks in gamma-ray bursts, Nature Commun. 6 (2015) 6783.

[78] M. G. Aartsen, K. Abraham, M. Ackermann, J. Adams, J. A. Aguilar, M. Ahlers, M. Ahrens, D. Altmann, T. Anderson, I. Ansseau, et al., An All-sky Search for Three Flavors of Neutrinos from Gamma-ray Bursts with the IceCube Neutrino Observatory, Astrophys. J. 824 (2016) 115.

[79] N. Senno, K. Murase, P. Meszaros, Choked Jets and Low-Luminosity Gamma-Ray Bursts as Hidden Neutrino Sources, Phys. Rev. D93 (2016) 083003.

[80] S. Razzaque, P. Meszaros, E. Waxman, High energy neutrinos from a slow jet model of core collapse supernovae, Mod. Phys. Lett. A20 (2005) 2351–2368.

[81] S. Ando, J. F. Beacom, Revealing the supernova-gamma-ray burst connection with TeV neutrinos, Phys. Rev. Lett. 95 (2005) 061103.

[82] I. Tamborra, S. Ando, Inspecting the supernova???gamma-ray-burst connection with high-energy neutrinos, Phys. Rev. D93 (2016) 053010.

[83] J. Hjorth, J. S. Bloom, The Gamma-Ray Burst - Supernova Connection, pp. 169–190.

[84] K. Murase, T. A. Thompson, E. O. Ofek, Probing Cosmic-Ray Ion Acceleration with Radio-Submm and Gamma-Ray Emission from Interaction-Powered Supernovae, Mon. Not. Roy. Astron. Soc. 440 (2014) 2528–2543.

[85] V. N. Zirakashvili, V. S. Ptuskin, Type IIn supernovae as sources of high energy astrophysical neutrinos, Astropart. Phys. 78 (2016) 28–34.

[86] R. Abbasi, et al., Searching for soft relativistic jets in core-collapse supernovae with the IceCube optical follow-up program, Astron. Astrophys. 539 (2012) A60.

[87] N. M. Law, et al., The Palomar Transient Factory: System Overview, Performance, and First Results, Publications of the Astronomical Society of the Pacific 121 (2009) 1395–1408.

[88] M. G. Aartsen, et al., The Detection of a SN IIn in Optical Follow-up Observations of IceCube Neutrino Events, Astrophys. J. 811 (2015) 52.

[89] M. G. Aartsen, et al., Very High-Energy Gamma-Ray Follow-Up Program Using Neutrino Triggers from IceCube, Submitted to: JINST (2016).

[90] M. Kadler, et al., Coincidence of a high-fluence blazar outburst with a PeV-energy neutrino event, Nature Phys. 12 (2016) 807–814.

[91] M. W. E. Smith, et al., The Astrophysical Multimessenger Observatory Network (AMON), Astropart. Phys. 45 (2013) 56–70.

[92] I. Collaboration, The IceCube Realtime Alert System, in preparation (2016).

[93] S. Adrian-Martinez, et al., High-energy Neutrino follow-up search of Gravitational Wave Event GW150914 with ANTARES and IceCube, Phys. Rev. D93 (2016) 122010.

[94] W. Baade, F. Zwicky, Cosmic Rays from Super-novae, Proceedings of the National Academy of Science 20 (1934) 259–263.

[95] F. W. Stecker, Diffuse Fluxes of Cosmic High-Energy Neutrinos, Astrophys. J. 228 (1979) 919–927.

[96] G. Domokos, B. Elliott, S. Kovesi-Domokos, Cosmic neutrino production in the Milky Way, J. Phys. G19 (1993) 899–912.

[97] V. S. Berezinsky, T. K. Gaisser, F. Halzen, T. Stanev, Diffuse radiation from cosmic ray interactions in the galaxy, Astropart. Phys. 1 (1993) 281–288.

[98] D. L. Bertsch, et al., Diffuse Gamma-Ray Emission in the Galactic Plane from Cosmic-Ray, Matter, and Photon Interactions, APJ 416 (1993) 587.

[99] G. Ingelman, M. Thunman, Particle production in the interstellar medium (1996).

[100] C. Evoli, D. Grasso, L. Maccione, Diffuse Neutrino and Gamma-ray Emissions of the Galaxy above the TeV, JCAP 0706 (2007) 003.

[101] D. Gaggero, D. Grasso, A. Marinelli, A. Urbano, M. Valli, The gamma-ray and neutrino sky: A consistent picture of Fermi-LAT, Milagro, and IceCube results, Astrophys. J. 815 (2015) L25.

[102] M. Ahlers, Y. Bai, V. Barger, R. Lu, Galactic neutrinos in the TeV to PeV range, Phys. Rev. D93 (2016) 013009.

[103] S. R. Kelner, F. A. Aharonian, V. V. Bugayov, Energy spectra of gamma-rays, electrons and neutrinos produced at proton-proton interactions in the very high energy regime, Phys. Rev. D74 (2006) 034018. [Erratum: Phys. Rev.D79,039901(2009)].

[104] M. M. Block, F. Halzen, Experimental Confirmation that the Proton is Asymptotically a Black Disk, Phys. Rev. Lett. 107 (2011) 212002.

[105] T. K. Gaisser, Atmospheric leptons, EPJ Web Conf. 52 (2013) 09004.

[106] G. L. Case, D. Bhattacharya, A new sigma-d relation and its application to the galactic supernova remnant distribution, Astrophys. J. 504 (1998) 761.

[107] M. Ahlers, K. Murase, Probing the Galactic Origin of the IceCube Excess with Gamma-Rays, Phys. Rev. D90 (2014) 023010.

[108] J. C. Joshi, W. Winter, N. Gupta, How Many of the Observed Neutrino Events Can Be Described by Cosmic Ray Interactions in the Milky Way?, Mon. Not. Roy. Astron. Soc. 439 (2014) 3414–3419. [Erratum: Mon. Not. Roy. Astron. Soc.446,no.1,892(2014)].

[109] M. Kachelrieß, S. Ostapchenko, Neutrino yield from Galactic cosmic rays, Phys. Rev. D90 (2014) 083002.

[110] F. Effenberger, H. Fichtner, K. Scherer, I. Busching, Anisotropic diffusion of galactic cosmic ray protons and their steady-state azimuthal distribution, Astron. Astrophys. 547 (2012) A120.

[111] D. Gaggero, L. Maccione, G. Di Bernardo, C. Evoli, D. Grasso, Three-Dimensional Model of Cosmic-Ray Lepton Propagation Reproduces Data from the Alpha Magnetic Spectrometer on the International Space Station, Phys. Rev. Lett. 111 (2013) 021102.

[112] M. Werner, R. Kissmann, A. W. Strong, O. Reimer, Spiral Arms as Cosmic Ray Source Distributions, Astropart. Phys. 64 (2015) 18–33.

[113] A. Neronov, D. V. Semikoz, C. Tchernin, PeV neutrinos from interactions of cosmic rays with the interstellar medium in the Galaxy, Phys. Rev. D89 (2014) 103002.

[114] A. Neronov, D. V. Semikoz, Evidence the Galactic contribution to the IceCube astrophysical neutrino flux, Astropart. Phys. 75 (2016) 60–63.

[115] S. Casanova, B. L. Dingus, Constraints on the TeV source population and its contribution to the galactic diffuse TeV emission, Astropart. Phys. 29 (2008) 63–69.

[116] J. M. Blondin, E. B. Wright, K. J. Borkowski, S. P. Reynolds, Transition to the Radiative Phase in Supernova Remnants, ApJ 500 (1998) 342–354.

[117] D. B. Fox, K. Kashiyama, P. Mészáros, Sub-PeV Neutrinos from TeV Unidentified Sources in the Galaxy, Astrophys. J. 774 (2013) 74.

[118] M. Mandelartz, J. Becker Tjus, Prediction of the diffuse neutrino flux from cosmic ray interactions near supernova remnants, Astropart. Phys. 65 (2015) 80–100.

[119] K. Fang, K. Kotera, K. Murase, A. V. Olinto, Testing the Newborn Pulsar Origin of Ultrahigh Energy Cosmic Rays with EeV Neutrinos, Phys. Rev. D90 (2014) 103005.

[120] P. Padovani, E. Resconi, Are both BL Lacs and pulsar wind nebulae the astrophysical counterparts of IceCube neutrino events?, Mon. Not. Roy. Astron. Soc. 443 (2014) 474–484.

[121] M. G. Aartsen, et al., Measurement of the cosmic ray energy spectrum with IceTop-73, Phys. Rev. D88 (2013) 042004.

[122] M. G. Aartsen, et al., Characterization of the Atmospheric Muon Flux in IceCube, Astropart. Phys. 78 (2016) 1–27.

[123] R. Abbasi, et al., Lateral Distribution of Muons in IceCube Cosmic Ray Events, Phys. Rev. D87 (2013) 012005.

[124] K. Rawlins, Cosmic ray spectrum and composition from three years of IceTop and IceCube, J. Phys. Conf. Ser. 718 (2016) 052033.

[125] R. Bellotti, et al., Simultaneous Observation of Extensive Air Showers and Deep Underground Muons at the Gran Sasso Laboratory, Phys. Rev. D42 (1990) 1396–1403.

[126] J. Ahrens, et al., Measurement of the cosmic ray composition at the knee with the SPASE-2/AMANDA-B10 detectors, Astropart. Phys. 21 (2004) 565–581.

[127] B. Peters, Primary cosmic radiation and extensive air showers, Nuovo Cimento XXII (1961) 800–819.

[128] K.-H. Kampert, M. Unger, Measurements of the Cosmic Ray Composition with Air Shower Experiments, Astropart. Phys. 35 (2012) 660–678.

[129] T. K. Gaisser, Primary spectrum and composition with IceCube/IceTop, in: Cosmic Ray International Seminar: The status and

the future of the UHE Cosmic Ray Physics in the post LHC era (CRIS 2015) Gallipoli, Italy, September 14-16, 2015.

[130] H. P. Dembinski, J. Gonzalez, Surface muons in IceTop, PoS ICRC2015 (2016) 267.

[131] A. Aab, et al., Muons in air showers at the Pierre Auger Observatory: Mean number in highly inclined events, Phys. Rev. D91 (2015) 032003. [Erratum: Phys. Rev.D91,no.5,059901(2015)].

[132] M. G. Aartsen, et al., Search for Galactic PeV Gamma Rays with the IceCube Neutrino Observatory, Phys. Rev. D87 (2013) 062002.

[133] M. G. Aartsen, et al., Search for Sources of High Energy Neutrons with Four Years of Data from the IceTop Detector, Astrophys. J. 830 (2016) 129.

[134] B. Bartoli, et al., Medium scale anisotropy in the TeV cosmic ray flux observed by ARGO-YBJ, Phys. Rev. D 88 (2013) 082001.

[135] R. Abbasi, et al., Measurement of the Anisotropy of Cosmic-ray Arrival Directions with IceCube, Astrophys. J. Lett. 718 (2010) L194–L198.

[136] R. Abbasi, et al., Observation of Anisotropy in the Arrival Directions of Galactic Cosmic Rays at Multiple Angular Scales with IceCube, Astrophys. J. 740 (2011) 16.

[137] M. Aartsen, et al., Observation of Cosmic-Ray Anisotropy with the IceTop Air Shower Array, Astrophys. J. 765 (2013) 55.

[138] M. G. Aartsen, et al., Anisotropy in Cosmic-ray Arrival Directions in the Southern Hemisphere Based on six Years of Data From the Icecube Detector, Astrophys. J. 826 (2016) 220.

[139] M. Aglietta, et al., Evolution of the Cosmic-Ray Anisotropy Above 10^{14} eV, Astrophys. J. Lett. 692 (2009) L130–L133.

[140] R. Abbasi, et al., Observation of Anisotropy in the Galactic Cosmic-Ray Arrival Directions at 400 TeV with IceCube, Astrophys. J. 746 (2012) 33.

[141] A. Abeysekara, et al., Observation of Small-scale Anisotropy in the Arrival Direction Distribution of TeV Cosmic Rays with HAWC, Astrophys. J. 796 (2014) 108.

[142] M. Amenomori, et al., Implication of the sidereal anisotropy of ˜5 TeV cosmic ray intensity observed with the Tibet III air shower array, American Institute of Physics Conference Series 932 (2007) 283.

[143] A. Abdo, et al., Discovery of Localized Regions of Excess 10-TeV Cosmic Rays, Phys. Rev. Lett. 101 (2008) 221101.

[144] M. Ahlers, P. Mertsch, Progress in Particle and Nuclear Physics (2016) in preparation.

[145] P. Abreu, et al., Search for first harmonic modulation in the right ascension distribution of cosmic rays detected at the Pierre Auger Observatory, Astropart. Phys. 34 (2011) 627–639.

[146] A. Chiavassa, et al., A study of the first harmonic of the large-scale anisotropies with the KASCADE-Grande experiment, Proc. 34th Int. Cosmic Ray Conference, The Hague, Netherlands (2015).

[147] M. Aartsen, et al., The IceCube Neutrino Observatory Part III: Cosmic Rays, Proc. 33rd Int. Cosmic Ray Conference, Rio de Janeiro, Brasil (2013).

[148] A. D. Erlykin, A. W. Wolfendale, The anisotropy of galactic cosmic rays as a product of stochastic supernova explosions, Astropart. Phys. 25 (2006) 183–194.

[149] P. Blasi, E. Amato, Diffusive propagation of cosmic rays from supernova remnants in the Galaxy. II: anisotropy, J. Cosmology Astropart. Phys. 1 (2012) 11.

[150] V. Ptuskin, Propagation of galactic cosmic rays, Astropart. Phys. 39 (2012) 44–51.

[151] M. Pohl, D. Eichler, Understanding TeV-band Cosmic-Ray Anisotropy, Astrophys. J. 766 (2013) 4.

[152] L. G. Sveshnikova, O. N. Strelnikova, V. S. Ptuskin, Spectrum and anisotropy of cosmic rays at TeV-PeV-energies and contribution of nearby sources, Astropart. Phys. 50 (2013) 33–46.

[153] M. Ahlers, Deciphering the Dipole Anisotropy of Galactic Cosmic Rays (2016).

[154] G. Giacinti, G. Sigl, Local Magnetic Turbulence and TeV-PeV Cosmic Ray Anisotropies, Phys. Rev. Lett. 109 (2012) 071101.

[155] P. L. Biermann, et al., Cosmic-Ray Transport and Anisotropies, Astrophys. J. 768 (2013) 124.

[156] M. Ahlers, Anomalous Anisotropies of Cosmic Rays from Turbulent Magnetic Fields, Phys. Rev. Lett. 112 (2014) 021101.

[157] M. Ahlers, P. Mertsch, Small-Scale Anisotropies of Cosmic Rays from Relative Diffusion, Astrophys. J. Lett. 815 (2015) L2.

[158] M. G. Aartsen, et al., IceCube-Gen2: A Vision for the Future of Neutrino Astronomy in Antarctica (2014).